Assessing Drying Shrinkage Induced Deterioration of Concrete Stored at Distinct Exposure Conditions

Xiangyu Zhu

A thesis submitted to the University of Ottawa in partial fulfillment of the requirements for the

MASTER OF APPLIED SCIENCE

in Civil Engineering

Under the supervision of Prof. Dr. Leandro Sanchez

Department of Civil Engineering

Faculty of Engineering

University of Ottawa

Abstract

Drying shrinkage is a damage mechanism that may potentially lead to the deterioration of concrete infrastructures. As the moisture content of concrete decreases over time, it undergoes a process of drying shrinkage, which subsequently induces a volume reduction, mass loss, and microcracks to the material. Although many studies and approaches to evaluate drying shrinkage have provided significant insights on the mechanism developments, the use of advanced microscopic techniques holds the potential for a more detailed and comprehensive evaluation of the generation and propagation of induced cracks. The damage rating index (DRI), a microscopic damage assessment protocol, has been proven to be an effective method to appraise and comprehend crack generation and propagation induced by the internal swelling reaction (ISR) mechanism. However, this procedure has never been used to assess shrinkage. Therefore, this work aims to assess the influence of relative humidity and temperature on the drying shrinkage mechanism and to assess the efficiency of using DRI to evaluate the deterioration of drying shrinkage on concrete according to the length change of concrete specimens with distinct exposure conditions. Furthermore, the cracks in cement paste (CCP) induced by drying shrinkage are investigated for the association with pores and interfacial transition zone (ITZ) in concrete.

Keywords: Drying shrinkage, relative humidity, microscopic techniques, damage rating index (DRI), cracks in the cement paste (CCP), interfacial transition zone (ITZ).

Acknowledgments

First of all, I am very thankful to my supervisor, Dr. Sanchez, who provided me with the opportunity of a Master of Applied Science (MASc.) in Civil Engineering at the University of Ottawa. I want to acknowledge and express my deepest gratitude to Dr. Sanchez, who helped and guided me throughout this research and taught me how to become a good researcher and what the truth of research is.

I also need to show my deepest respect to my mentor, Olusola Olajide, who helped me comprehend the project and strongly supported me in this research and the various lab works. I am very thankful for your persistence and dedication.

I also acknowledge all the appreciated help, support, and advice provided by Rennan Medeiros, who taught me the better presentation of statistical information derived from my dataset.

I really appreciate every one of my colleagues in the μStructure group. I would like to thank Cassandra Trottier, who taught me many things in the lab and got funds from the collaboration with Englobe Corp. I am thankful to Zichun Xia, Haixu Zhang, Leah Kristufek, and Ana Bergmann for their help with the experiments in my projects.

Last but not least, I am thankful for my parents, Guangli Zhu and Min Gu. Even though I have been away from my home for 5 years and could not go back home during COVID-19, they support me to do what I think is right without hesitation and doubts.

Table of Contents

List of Figures

List of Tables

Symbols/ Abbreviations

AAR	Alkali-Aggregate Reaction
ASR	Alkali-Silica Reaction
CAD	Coarse Aggregate Debonded
CCA	Cracks in Coarse Aggregate
CCP	Cracks in Cement Paste
CCPG	Cracks with Reaction Product in Cement Paste
CRD	Comparator Reading
CSH	Calcium Silicate Hydrate
DAP	Disaggregate/ Corroded Aggregate Particle
DEF	Delayed Ettringite Formation
DICM	Digital Image Correlation Method
DRI	Damage Rating Index
FEIM	Fluorescent Epoxy Impregnation Method
FT	Freezing and Thawing Cycles
HCP	Hydrated Cement Paste
ISR	Internal Swelling Reaction
ITZ	Interfacial Transition Zone
NSC	Normal Strength Concrete
OCA	Opened Cracks in Coarse Aggregate
OCAG	Opened Cracks with Reaction Product in Coarse Aggregate
RH	Relative Humidity
W/C	Water-to-Cement Ratio

1. Chapter One: Introduction

1.1 Drying Shrinkage in Concrete

Concrete is a porous material made of aggregate particles embedded a cement paste. It is prone to capillary water loss when exposed to a drier condition as a result of disparities in humidity levels between the concrete and the environment [1–5]. This occurrence triggers a reduction in volume, commonly referred to as drying shrinkage. The presence of aggregate particles within the cement paste imposes limitations on the extent of contraction, resulting in the development of cracks within the cement paste, particularly at the interfacial transition zone (ITZ) [4, 6]. Drying shrinkage-induced deterioration in concrete is typically influenced by concrete features (e.g., water-to-cement ratio, cement content and size of coarse aggregate and environmental factors such as, temperature and relative humidity[1–8]. Water plays a critical role in drying shrinkage due to its relationship with the volume and properties of capillary pores in concrete; a high water-cement ratio leads to a high initial volume of capillary pores within the concrete matrix [4, 8]. As water evaporates from these pores during drying, especially when the external relative humidity is lower, the concrete undergoes greater contraction leading to a pronounced drying shrinkage [1, 9].

Drying shrinkage causes cracks in concrete which can compromise its structural integrity, and impact durability. Drying shrinkage-induced cracks can allow the ingress of moisture, chemicals, and other aggressive substances into the concrete, leading to durability challenges, such as corrosion, alkali-silica reaction (ASR), and freeze-thaw damage, significantly reducing the lifespan of concrete structures [11].

1.2 Microstructure Assessment of Drying Shrinkage

Drying shrinkage is a crucial factor that has a substantial impact on the long-term performance of concrete structures. The assessment of microstructure has emerged as crucial for gaining insights into the underlying mechanisms of various durability issues, such as drying shrinkage in concrete. This evaluation has been prominently conducted using tools such as scanning electron microscopy (SEM). This tool offers micrographs at a significantly high magnification level which has successfully been used to assess the interfacial transition zone (ITZ), hydration products, and other properties of the concrete microstructure [12]. Numerous researchers have explored the mechanism of drying shrinkage using SEM. Although SEM is a powerful tool for high-resolution imaging and microanalysis[13], it does come with its limitations. SEM can visually and qualitatively/semi-quantitatively represent microcracks and chemical products, such as calcium silicate hydrate (CSH), within the hydrated cement paste and interfacial transition zone (ITZ). However, it lacks a quantitative way of assessing the significance of the information conveyed by these images. The damage rating index (DRI), which is well-known as the one of semi-quantitative methods for the microstructure of concrete, has been proven to effectively evaluate the damage induced by the internal swelling reaction (ISR) according to the expansion level [14]. The proposed method can summarize the distinct characteristics of cracks observed in distressed concrete. Additionally, it assigns specific weighting factors to different types of cracks, enabling the calculation of a damage rating index. In recent years, significant success has been made in the development of the DRI to effectively evaluate the extent of internal swelling reaction (ISR) mechanisms, such as Alkali-silica reaction (ASR) delayed ettringite formation (DEF) and freezing and thawing

cycles (FT) [6, 14, 15]. However, this method has never been used to assess drying shrinkage. This work aims to assess the potential of the DRI as a diagnostic protocol to appraise drying shrinkage damage in concrete exposed to a number of relative humidity conditions.

1.3 Research Objectives and Scope of Work

The goal of the research is to assess the potential use of the damage rating index (DRI) to assess drying shrinkage-induced cracks in concrete stored at different moisture conditions. First, the laboratory-made concrete specimens containing non-reactive aggregates (i.e., reactive to alkali-aggregate reaction) are fabricated and stored in distinct moisture conditions (100%, 90%, 82%, 75%, 62%) and temperatures (21℃, 38℃, and 60℃). Length and mass change were monitored over six months. During the conditioning period, the dynamic resonance frequency is utilized to measure the dynamic elastic modulus. After 6 months of conditioning and periodical measurements, the porosity test was performed to correlate the porosity and drying shrinkage. Subsequently, microscopic evaluations of the specimens were conducted utilizing the DRI technique to determine induced cracks by drying shrinkage in concrete. Finally, the DRI outputs were compared with the other outcomes measured.

1.4 Organization of Thesis

This thesis was divided into five chapters. The first chapter represents the introduction of the thesis, which describes the cause and influence of drying shrinkage in concrete as well as briefly describes the microstructure assessment technique known as the damage rating index (DRI). The second chapter is the literature review of drying shrinkage. It first explains the cause of this mechanism in concrete; then, it describes factors influencing

drying shrinkage, such as water-to-cement ratio, relative humidity, and temperature. Meanwhile, it explains the effects of drying shrinkage on the mechanical properties and microstructure of concrete from existing research studies. The third chapter aims to evaluate the development in concrete under various exposure conditions. Furthermore, it analyzes the influence of drying shrinkage on the porosity and dynamic elastic modulus. The fourth chapter of the thesis is the microstructure assessment of drying shrinkage-induced deterioration via the DRI. This chapter assesses the efficiency of the DRI in evaluating drying shrinkage. The fifth chapter gives a comprehensive summary of the findings and impacts, as well as recommendations for potential future research efforts within the field. Lastly, in all work mentioned in the thesis, the laboratory work measurements, sample preparation, microscopic and data analysis (with the help of Olusola Olajide, Ph.D. Candidate), the reviewing and advising of the thesis (with the help of Olusola Olajide, Ph.D. Candidate, and Rennan Medeiros, Ph.D. Candidate), and the writing of the thesis were conducted by me. My supervisor, Dr. Leandro Sanchez, has made significant contributions to the data analysis and review processes of this thesis.

1.5 References

[1] R. K. Mishra, R. K. Tripathi, and V. Dubey, “Early age shrinkage pattern of concrete on replacement of fine aggregate with industrial by-product,” *Journal of Radiation Research and Applied Sciences*, vol. 9, no. 4, pp. 386–391, Oct. 2016, doi: 10.1016/j.jrras.2016.05.003.

[2] B. Bissonnette, P. Pierre, and M. Pigeon, “Influence of key parameters on drying shrinkage of cementitious materials,” *Cement and Concrete Research*, vol. 29, no. 10, pp. 1655–1662, Oct. 1999, doi: 10.1016/S0008-8846(99)00156-8.

[3] S. Nuhu, S. Ladan, and A. U. Muhammad, "Effects and Control of Chemical Composition of Clinker for Cement Production," *International Journal of Control Science and Engineering*, vol. 10, no. 1, pp. 16–21, 2020, doi: 10.5923/j.control.20201001.03.

[4] P. K. Mehta and P. J. M. Monteiro, *Concrete: microstructure, properties, and materials*, 3rd ed. New York: McGraw-Hill, 2006.

[5] A. M. Neville and J. J. Brooks, *Concrete Technology*, Second Edition.

[6] L. F. M. Sanchez, T. Drimalas, and B. Fournier, "Assessing condition of concrete affected by internal swelling reactions (ISR) through the Damage Rating Index (DRI)," *Cement*, vol.1–2, p.100001, Jun. 2020, doi: 10.1016/j.cement.2020.100001.

[7] J. Yang, Q. Wang, and Y. Zhou, "Influence of Curing Time on the Drying Shrinkage of Concretes with Different Binders and Water-to-Binder Ratios," *Advances in Materials Science and Engineering*, vol. 2017, pp. 1–10, 2017, doi: 10.1155/2017/2695435.

[8] Y. Z. Yang, M. G. Li, H. W. Deng, and Q. Liu, "Effects of Temperature on Drying Shrinkage of Concrete," *AMM*, vol. 584–586, pp. 1176–1181, Jul. 2014, doi: 10.4028/www.scientific.net/AMM.584-586.1176.

[9] B. Al-Shathr, A. Abdulameer, and T. al-Attar, "The role of ambient temperature variation on drying shrinkage development of self-compacting Portland-limestone cement concrete," *MATEC Web Conf.*, vol. 162, p. 02021, 2018, doi: 10.1051/matecconf/201816202021.

[10] I. Maruyama, “Origin of Drying Shrinkage of Hardened Cement Paste: Hydration Pressure,” *ACT*, vol. 8, no. 2, pp. 187–200, Jun. 2010, doi: 10.3151/jact.8.187.

[11] L. F. M. Sanchez, B. Fournier, M. Jolin, D. Mitchell, and J. Bastien, “Overall assessment of Alkali-Aggregate Reaction (AAR) in concretes presenting different strengths and incorporating a wide range of reactive aggregate types and natures,” *Cement and Concrete Research*, vol. 93,pp. 17–31, Mar. 2017, doi: 10.1016/j.cemconres.2016.12.001.

[12] T. Akçaoğlu, M. Tokyay, and T. Çelik, “Assessing the ITZ microcracking via scanning electron microscope and its effect on the failure behavior of concrete,” *Cement and Concrete Research*, vol. 35, no. 2, pp. 358–363, Feb. 2005, doi: 10.1016/j.cemconres.2004.05.042.

[13] Z. Ikhlasi, A. Gholampour, and T. Vincent, “Drying shrinkage of waste-based concrete reinforced with pristine graphene (PRG) nanomaterial,” *Materials Today: Proceedings*, p.S2214785323029176,May 2023, doi: 10.1016/j.matpr.2023.05.287.

[14] L. Sanchez, B. Fournier, M. Jolin, J. Bastien, D. Mitchell, and M. Noel, ‘The Use of the Damage Rating Index (DRI) for The Condition Assessment of Aging Distressed Concrete’, in *16th International Conference on Alkali-Aggregate Reaction*, Brazil, 2016.

[15] L. F. M. Sanchez, T. Drimalas, B. Fournier, D. Mitchell, and J. Bastien, “Comprehensive damage assessment in concrete affected by different internal swelling reaction (ISR) mechanisms,” *Cement and Concrete Research*, vol. 107, pp. 284–303, May 2018, doi: 10.1016/j.cemconres.2018.02.017.

2. Chapter Two: Literature Review: Drying Shrinkage in Concrete

2.1 Introduction of Drying Shrinkage in Concrete

Shrinkage in concrete manifests the contraction of the volume of concrete; it can be affected by the loss of water by evaporation, hydration reaction and carbonation. Therefore, the shrinkage behaviour of concrete and the influencing factors cause different types of shrinkage, such as plastic shrinkage, autogenous shrinkage, drying shrinkage, carbonation shrinkage, and thermal shrinkage [1]. Drying shrinkage is the water loss from the evaporation in the hardened state of concrete. It often commences in the early age of concrete and persists over several months [2, 5]. A correlation between the paste volume content and the weight loss per unit volume, as well as the relationship between drying shrinkage and weight loss in the concrete, is illustrated in Figure 2.1. The findings indicate a direct proportionality between weight loss per unit volume of material and paste volume for both water-to-cement (W/C) ratios [4]. A larger W/C ratio results in greater weight loss, mostly due to the increased presence of free water [4]. In mixes characterized by a water-to-cement (W/C) ratio of 0.35, the extent of shrinkage is seen to exhibit a proportionate relationship with the amount of water lost [4]. In the scenario with the 0.50 water-to-cement ratio, the minimal shrinkage resulting from the initial drying phase can be attributed to the water primarily originating from the larger capillary holes [2].

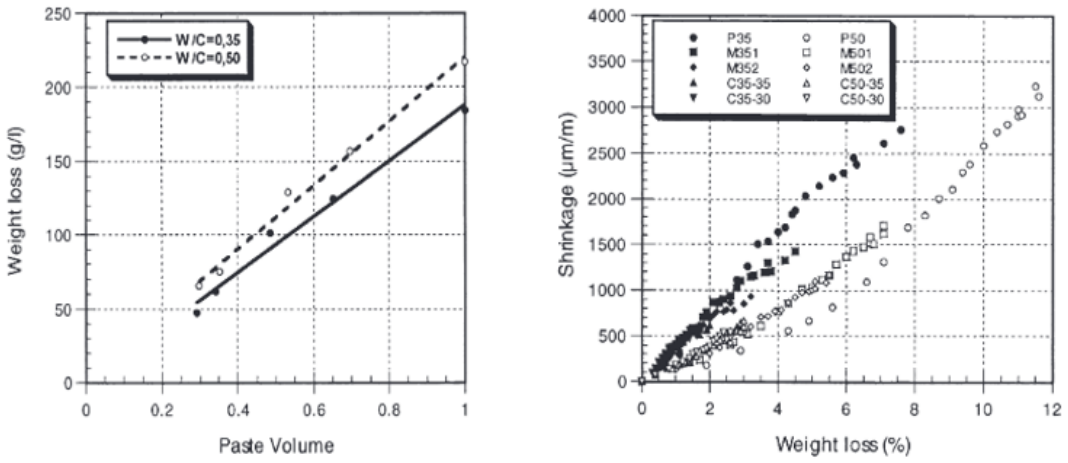

(a) (b)

Figure 2.1 Relation Between Weight Loss Per Unit Volume and Paste Volume (a) and Relation Between Shrinkage and Weight Loss (b) [4]

Furthermore, the tensile stress induced by loss of moisture in drying shrinkage causes the formation and propagation of cracks in the concrete because the aggregate in the concrete restricts the occurrence of volume contraction of cement paste due to drying shrinkage [2–4]. The drying shrinkage in concrete is believed to be primarily caused by the loss of capillary water and adsorbed water from the hydrated cement paste; meanwhile, the contraction of the system during drying can be linked to the loss of water trapped under hydrostatic tension within minuscule capillaries measuring less than 50 nm in the hydrated cement paste [2]. Therefore, the saturated cement paste can't maintain dimensional stability when exposed to the low relative humidity environment because the shrinkage is caused by the consumption of adsorbed water from the calcium silicate hydrate (CSH) phase [2].

The behaviour of concrete during the processes of drying and rewetting is illustrated in Figure 2.2. The phenomenon of drying shrinkage in concrete demonstrates a certain level of irreversibility. The data presented in Figure 2.2 demonstrates that upon rehydration, the

concrete did not fully regain its initial dimensions during the initial drying process. Drying shrinkage has been separated into two distinct categories: reversible shrinkage, which refers to the portion of total shrinkage that can be consistently repeated during wet-dry cycles, and irreversible shrinkage, which denotes the portion of total shrinkage that occurs during the initial drying process and cannot be replicated in subsequent wet-dry cycles; in addition, the phenomenon of irreversible drying shrinkage is likely attributed to the formation of chemical bonds within the calcium silicate hydrate (CSH) structure as a result of the drying process.

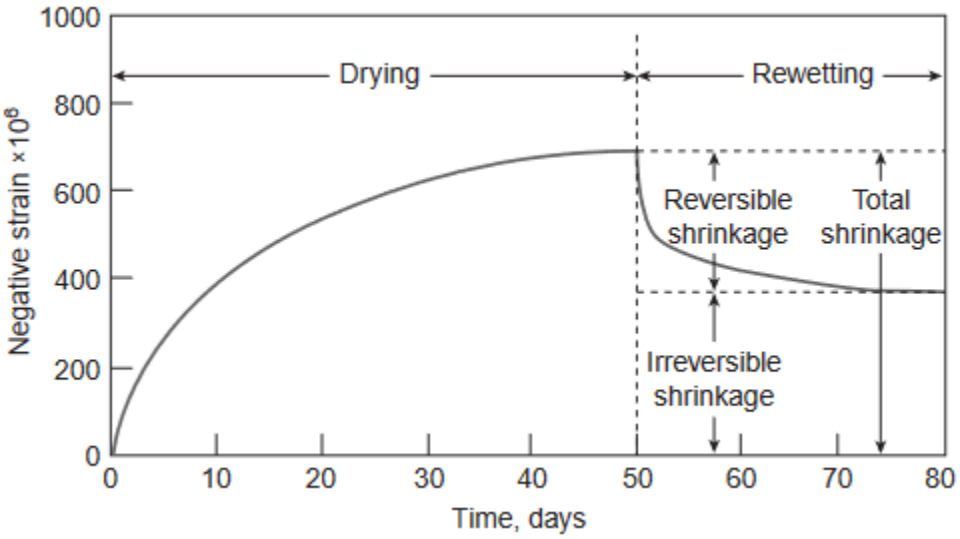

Figure 2.2 Reversibility of Drying Shrinkage [2]

2.2 Effect of Drying Shrinkage in Concrete

Concrete made of Portland cement is known to be highly susceptible to drying shrinkage due to its poor tensile strength [7]. The phenomenon of drying shrinkage typically results in the occurrence of cracking and volume contraction [7–9]. Meanwhile, it is commonly seen that the likelihood of durability issues increases. Both the strength and the

permeability of the hydrated cement paste are inversely correlated with the connection of the pores, which also affects the microstructure of the concrete, such as the hydrated cement paste and interfacial transition zone (ITZ). Meanwhile, several research studies have also proved that drying shrinkage is a physical mechanism that induces the loss of mechanical properties of concrete construction [10–12].

2.2.1 Drying Shrinkage on Hydrate Cement Paste (HCP)

Hydrated cement paste contains four solid phases, which are Calcium silicate hydrate (CSH), Calcium hydroxide (portlandite), Calcium sulfoaluminates hydrate, and anhydrous clicker particles [5]. Meanwhile, the hydrated cement paste comprises many sorts of voids (interlayer space in CSH, capillary voids, and air voids) that induce drying shrinkage when there is a loss of water. Also, the degree of hydration represents the percentage of cement that has reacted with water and formed hydrated compounds. It is an essential factor in determining the strength of the concrete.

Capillary voids present the space that is not occupied by the cement or the products of hydration. The original spacing between the anhydrous cement particles in the freshly mixed cement paste and the degree of hydration affects the volume and size of the capillary voids [6]. In addition to vapour in empty or partially water-filled voids, several types of water are defined, including capillary water, absorbed water, interlayer water, and chemically bonded water. Drying shrinkage is caused by the loss from capillary water (when the relative humidity is less than the cement past humidity), absorbed water (when the relative humidity is less than 30%), and interlayer water (when the relative humidity is less than 10%); in addition, chemically bonded water does not affected by drying[2]. Compared with the absorbed water, the capillary water is not affected by the attractive

force generated by the solid surface. Also, the pore size of capillary voids is significant because the water loss only occurred in the small capillary pore (5 to 50 nm) impacts the drying shrinkage; otherwise, free water does not affect the volume change [2, 4].

Figure 2.3 states the decrease in capillary porosity is affected by either the decrease in the water-to-cement ratio or an increase in the degree of hydration; also, with the reduction of capillary porosity, the strength of hydrated cement pastes increases because of a high degree of hydration [4].

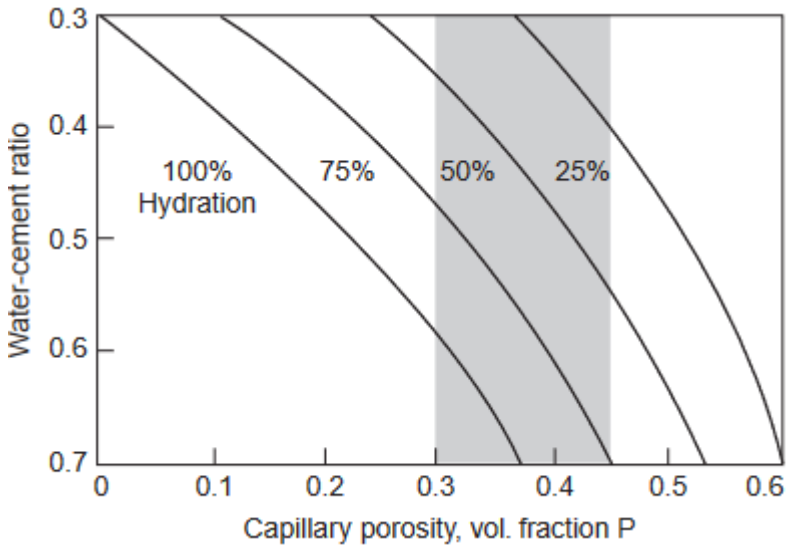

Figure 2.3 Influence of Water-Cement Ratio and Degree of Hydration on Capillary Porosity [4]

The loss of capillary water due to drying shrinkage causes the reduction of the disjoining pressure when the hydrated cement paste is saturated and exposed under low moisture conditions. Meanwhile, drying shrinkage also affects the loss of the absorbed water and compressive stress on the solid walls of the capillary pore due to the hydrostatic tension exerted by water in small capillaries.[4].

2.2.2 Drying Shrinkage on Interfacial Transition Zone (ITZ)

A good description of the formation and microstructure of concrete ITZ is concluded and Figure 2.4 shows the difference in size and distribution of three types of chemical compounds between the ITZ and bulk cement paste [2, 11].

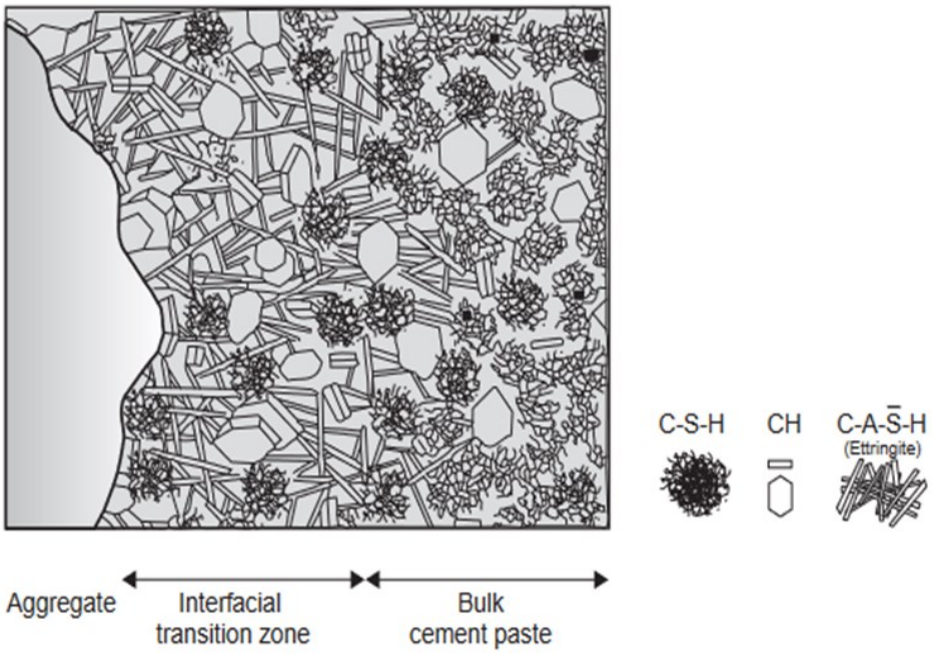

Figure 2.4 Diagrammatic Representation of the Interfacial Transition Zone and Bulk Cement Paste In Concrete [2]

The larger size and volume of void appear in the ITZ than in the bulk cement paste at the early age contributing to the low strength of the ITZ. The ITZ limits the strength of concrete since it is the weakest phase in the system. The initiation of cracks occurs due to the stress concentrations at large voids in the matrix when the stress level is higher than about 70% of the ultimate compressive strength [2]. When the drying shrinkage occurs in the ITZ, the cracks progressively grow and they orient and join to the cracks at ITZ with increasing stress [6]. The factors influencing the microcracks depend on the aggregate, the cement

content, the water-to-cement ratio, the degree of hydration, temperature, and relative humidity. The type and quality of aggregates used in concrete can affect its overall strength and durability. Aggregates with a high degree of reactivity minerals can lead to microcracking. Cement increases concrete matrix density and strength, decreasing microcracks, but excess cement might also cause thermal cracking during hydration. A lower water-to-cement ratio generally results in stronger and less porous concrete, which is less prone to microcracking. Temperature and relative humidity can significantly impact the development of microcracks by affecting the exposure conditions of concrete.

Meanwhile, the drying shrinkage on ITZ affects the durability of concrete. If the concrete is under identical conditions, the higher local water-cement ratio in the interfacial transition zone causes ITZ to become more porous and attain lower strength, compared to the bulk cement paste. When the microcracks occur at ITZ, the permeability of the concrete is increased and the possibility of a chemical attack on the concrete is increased[2].

2.2.3 Mechanical Properties Influenced by Drying Shrinkage

Through experimental analysis on a wall-type micro-reinforced concrete (RC) structure, which was designed to replicate a section of a nuclear reactor building, drying shrinkage affects the stiffness of the structure but does not have any influence on its ultimate loading capacity [2]. In addition, numerical investigation is applied to examine the influence of drying-induced cracking on the alteration of stiffness in a reinforced concrete pier by using the finite element; as a result, the study revealed that the stiffness was impacted by shrinkage-induced cracking, while the ultimate loading capacity remained unaffected [11].

Significantly, the comprehensive investigation utilizing a rigid-body spring network model showed that the drying shrinkage strain of concrete resulted in an escalation of crack width,

thus leading to a decrease in the overall strength of the concrete within the structure [12]. The influence of drying on the compressive strength of concrete is determined by the specific alteration in the strength of hardened cement paste resulting from its colloidal properties; however, it is also influenced by the overall shrinkage of the material, which alters the extent of damage in concrete during the drying process [2]. Since the tensile stress induced by drying shrinkage occurs at both bulk cement paste and ITZ of concrete, this phenomenon initiates microcracks when this tensile stress exceeds the tension strength of concrete. On the other hand, the formation and propagation of microcracks id developed rapidly at a low level of compressive stress level as well.

In addition, Figure 2.5 illustrates that the flexural cracking load on the concrete beam with the drying condition exhibited an apparent reduction in comparison to the sealed beams. It states that this discrepancy can be attributed to the increase of tensile stress resulting from the drying shrinkage of the concrete; meanwhile, it was noted that the application of stresses caused by drying shrinkage had a dual effect on reinforced concrete beams, leading to a decrease in both stiffness and the load at which diagonal cracking occurred [13].

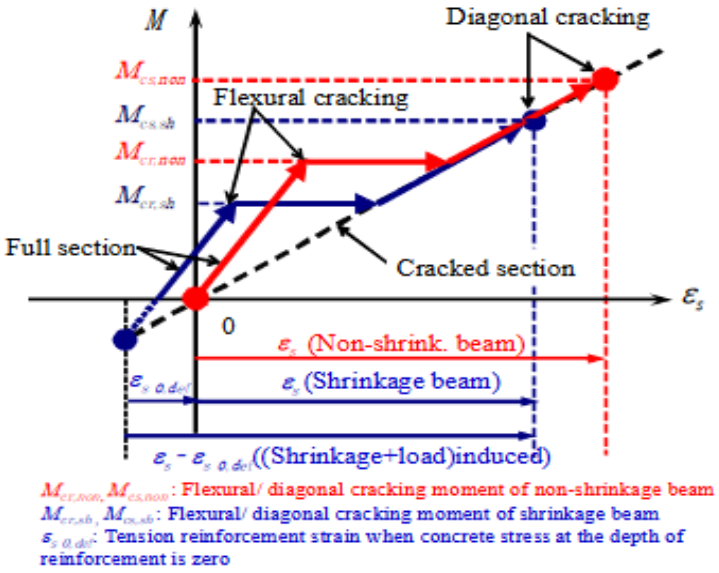

Figure 2.5 Concept of Strain Change in Tension Reinforcement Due to Drying Shrinkage [13]

2.3 Factors Influencing Drying Shrinkage

The rate of drying shrinkage in concrete is primarily influenced by ambient factors, specifically the relative humidity and temperature in the surrounding environment. In addition, it should be noted that several specific factors, including the water-to-cement ratio, type of cement, aggregate features, and the incorporation of admixtures, exert a substantial impact on the magnitude of drying shrinkage [2, 3, 15–20].

2.3.1 Water to Cement Ratio (w/c)

As mentioned earlier, the water-to-cement (w/c) ratio represents the ratio of water components to cement components in concrete. Lower w/c ratios usually result in denser and stronger concrete with enhanced durability due to reduced permeability. The increase in the water-to-cement ratio could increase drying shrinkage[2, 13]. Meanwhile, a higher water-to-cement ratio signifies a higher volume of capillary pores in both hydrated cement

paste and the interfacial transition zone of concrete [10]. As shown in Figure 2.6, at the same degree of hydration, the presence of the concrete mixture with a high w/c ratio not only increases the total volume of the hydrated cement paste but also illustrates an increased number of capillary pores, thereby increasing the porosity of the concrete. The high porosity means an increased number of voids through which water can lose to the low moisture environment, thereby leading to many more pronounced drying shrinkage behaviours. For instance, the process of water evaporation can induce volumetric contraction of concrete and potentially result in cracking due to internal tensions due to drying shrinkage.

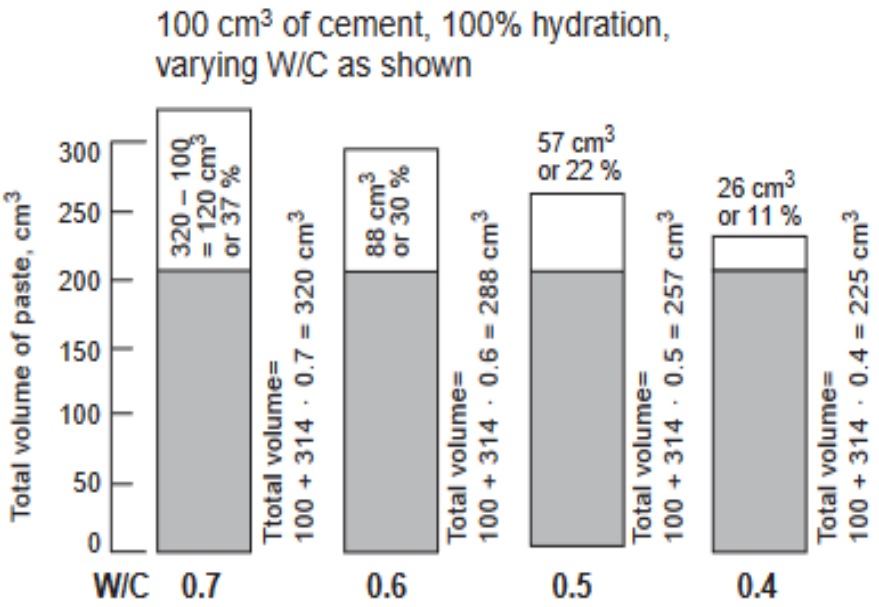

Figure 2.6 Changes in the Capillary Porosity with Varying Water-Cement Ratio [2]

2.3.2 Temperature

Temperature affects the rate of water evaporation from the concrete; also, temperature accelerates the chemical reaction in the concrete mixtures, impacting the degree of

hydration [2]. It revealed that the rise of temperatures accelerates the drying shrinking process; furthermore, Figure 2.7 illustrates that the drying shrinkage of concrete exhibits an initial period of rapid development during early ages, followed by a stable performance in the later stages; also, the impact of the water-cement ratio on the drying shrinkage of concrete is diminishing with the rise of temperature [19].

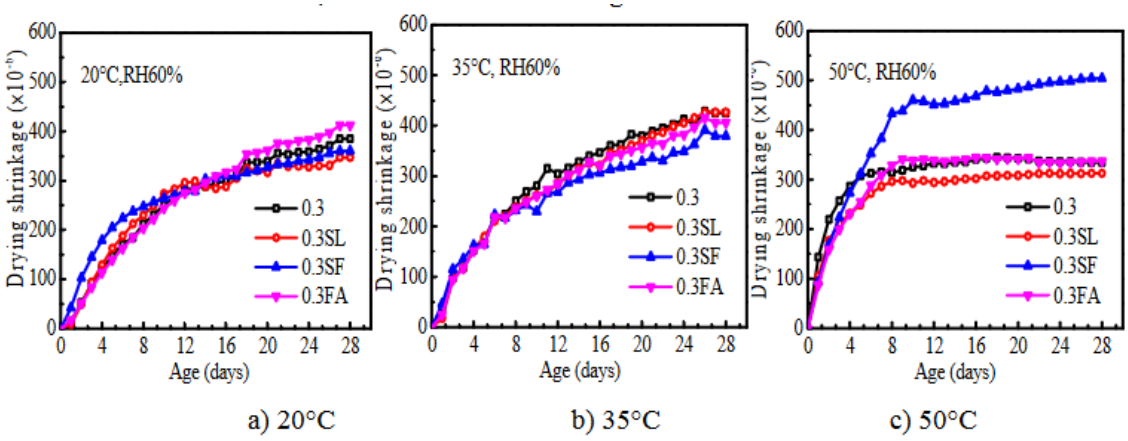

Figure 2.7 Effects of Mineral Admixture on Drying Shrinkage of Concrete[19]

Furthermore, temperature is one of the significant roles in the casting, curing, and placing the concrete [2]. Under the identical condition of the concrete, the concrete with high-temperature casting causes a lower strength; also, if the curing temperature is lower it will be the strength up to 28 days slower. Hence, in comparison to the strength exhibited by specimens cured under standard laboratory temperature conditions, the in situ concrete strength demonstrates an increase during the initial stages and a decrease during the later stages [2].

2.3.3 Relative humidity

The relative humidity of the concrete is the driving force influencing the drying shrinkage. Saturated hydrated cement paste is not dimensionally stable. As long as it is held at 100

percent relative humidity (RH), practically no dimensional change occurs; however, when exposed to environmental humidity, which normally is much lower than 100 percent, the material begins to lose water and shrink [2]. Also, the relative humidity of the ambient environment impacts the degree of hydration of the concrete. In the laboratory or work field, drying begins either after demolding or at the finish of the curing period to establish an equilibrium between the water content in the concrete and the surrounding atmosphere. This equilibrium means the moisture content in the concrete tends to gradually reach a balance with the ambient conditions. Also, the rate of drying in this particular process is characterized by significant slowness, often failing to achieve this equilibrium within the intended operational lifespan [21].

Figure 2.8 illustrates that drying shrinkage behaves inversely with the relative humidity of air [2] . Drying shrinkage at low relative humidity primarily arises from the alteration of surface free energy of the hydration products; conversely, shrinkage at high relative humidity is sensitive to the disjoining pressure [2,20–21].

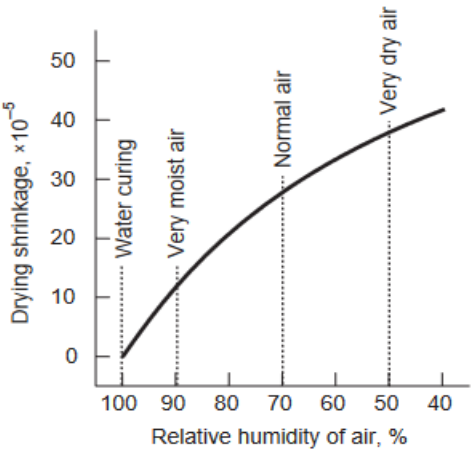

Figure 2.8 Influence of The Relative Humidity on Drying Shrinkage [2]

Significantly, compared to the capillary water that is lost when exposed to the ambient environment, absorbed water and interlayer water are removed when the relative humidity of concrete is lower than 30% and 10%, respectively [2]. On the other hand, no loss of chemically bonded water is observed due to shrinkage.

2.4 Standardized Test for Drying Shrinkage in Concrete

ASTM C157-17 is the standardized test to measure the length change due to drying shrinkage in hardened concrete [22]. The length change (ΔL_x) is measured by the gages set at the ends of the prism. The initial comparator readings (CRD) are taken 4 hours after the curing condition at 23 $\pm$ 0.5 °C. After the initial comparator reading, these specimens are stored in lime-saturated water at 23 $\pm$ 2 °C until 28. At the end of the curing period, the second comparator readings are taken after the specimens are under the controlled temperature. In this test, the concrete specimens are frequently immersed in the lime-saturated water for storage; further readings on length changes of specimens are required following the end of the curing process at intervals of 4, 7, 14, and 28 days, as well as 8, 16, 32, and 64 weeks. The formula for the length change is shown as follows [22]:

$\Delta L_x = \frac{CRD - CRD_{initial}}{G} * 100$, where G means the gage length.

2.5 Microscopic Assessment of Drying Shrinkage

The microscopic study of concrete plays an indispensable role in understanding its microstructure, diagnosing problems, optimizing mix designs, and advancing research in concrete technology. Therefore, many microscopic methods have been developed and widely used to bridge the gap between the macroscopic performance of concrete structures

and the underlying microstructure phenomena. It is integral to the ongoing efforts to improve and innovate within the field of concrete technology.

2.5.1 Scanning Electron Microscope (SEM)

SEM is widely used to investigate the drying shrinkage behaviour of concrete. SEM can provide micrographs at a significantly high magnification level (e.g., magnification of 6000 and 20000) to assess the correlation between the interfacial transition zone (ITZ) and the strength of mortar under various conditions [10]. It can generate high-solution images to observe the microcracks with different widths and depths in concrete in the cement paste [23].SEM analysis can assess the microstructural morphology of concrete mixtures; Figure 2.9 clearly illustrates the morphology of microcracking and capillary pores from waste-based concrete influenced drying shrinkage by SEM [24].

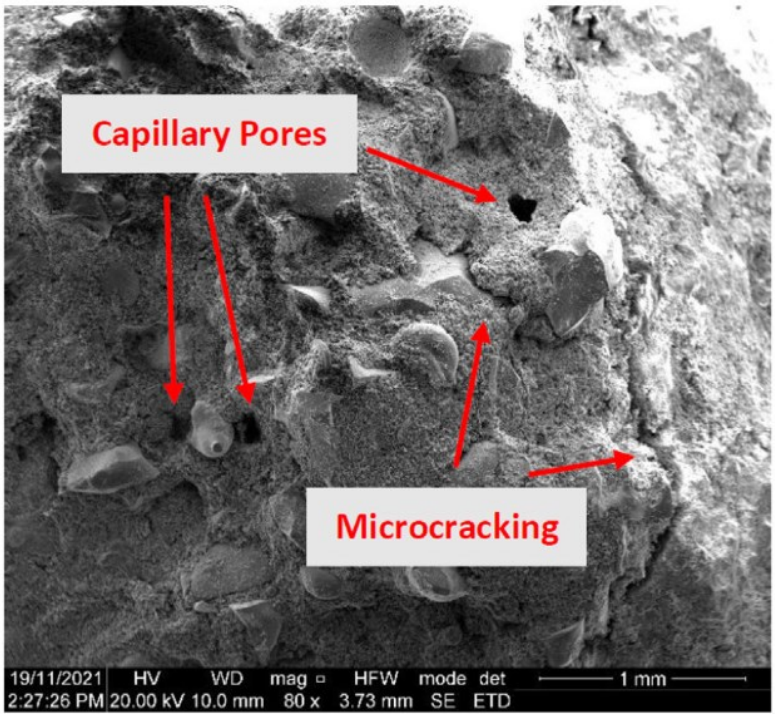

Figure 2.9 Observing Microcracking and Capillary Pores by SEM

2.5.2 Fluorescent epoxy impregnation (FEI) with Digital Image Correlation Method (DIC)

DIC has been used to assess the drying shrinkage of aging concrete specimens. The samples are impregnated with fluorescence epoxy before obtaining the images. The polished epoxy-impregnated samples make the distribution of the crack due to shrinkage visible (Figure 2.10) [25]. DIC reveals alterations in strain distributions, the maximum principal strain distribution exhibited expansive strains, despite the overall contraction of the entire specimen; moreover, the significant expansion was particularly observed in concrete samples exhibiting minimal drying shrinkage (Figure 2.10 b) [25].

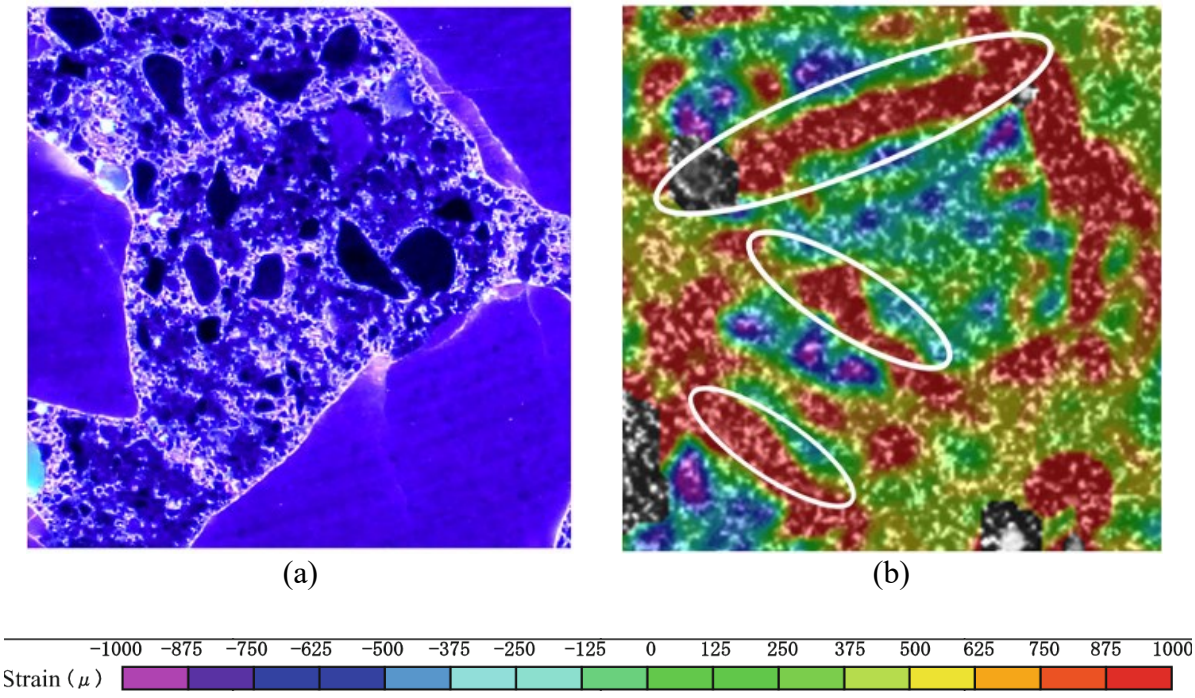

Figure 2.10 Comparison of Image Obtained with FEIM (a) And Magnified Images of Maximum Principal Strain Distribution (b) [25]

2.5.2 Damage Rating Index (DRI)

DRI is a semi-quantitative microscopic method that has prominently been used to assess damage in concrete through the DRI number and crack features for distinct mechanisms

[26]–[28]. The DRI is capable of comprehensively evaluating the influence of distressed concrete, which can be applied to assess the internal swelling reaction (ISR) mechanisms, such as the alkali-silica reaction (AAR), delayed ettringite formation (DEF), and freeze-thaw (FT) cycles [27]. The distress features are quantified by examining 1-centimeter squares on the polished concrete surface as illustrated in Figure 2.11(a), using a stereomicroscope set at a magnification level of 16x; then, the damage features are subsequently multiplied by weighting factors shown in Figure 2.11(b), based on the respective significance concerning the associated distress mechanism. The DRI output can be used to describe the damage in affected concrete as shown in Figure 2.11(c). [26–31].

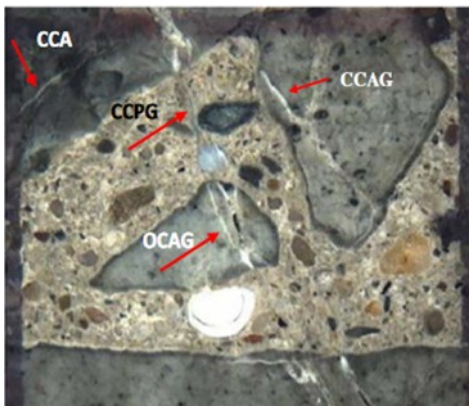

(a)

Petrographic features	Abbreviation	Weighing factor
Cracks in coarse aggregate	CCA	0.25
Opened cracks in coarse aggregates	OCA	2
Crack with reaction product in coarse aggregate	OCAG	2
Coarse aggregate debonded	CAD	3
Disaggregate/corroded aggregate particle	DAP	2
Cracks in cement paste	CCP	3
Cracks with reaction product in cement paste	CCPG	3

(b)

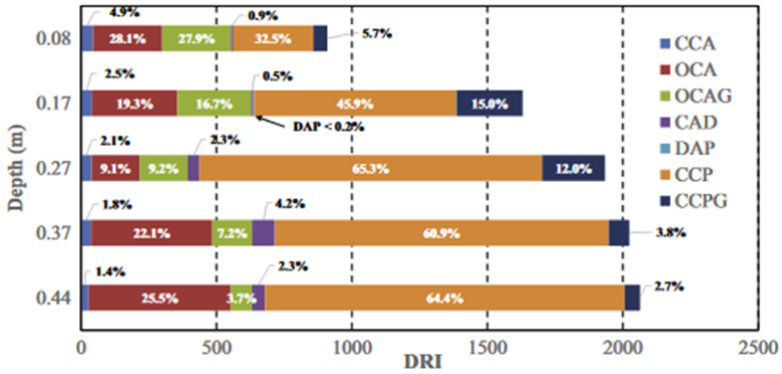

(c)

Figure 2.11 DRI Method: (a) $1\,cm^2$ Section Highlighting the Most Common Distress Features Displayed; (b) Damage Features and Respective Weighing Factors [26]; (c) DRI results [30]

Fracture mechanics adequately describes the generation and propagation of distress in porous materials such as concrete [26]. Cracks form and propagate according to the minimum energy principle, which states that the release of elastic energy happens with minimal fracture energy. This means that cracks often choose the shortest paths to propagate, which in cement paste combinations means going through the interfacial transition zone in mortar or concrete mixes [26]. Also, cracks can sometimes take faster routes within the aggregate particles instead of propagating along the aggregates if this path

is energetically shorter; it takes place when the aggregate particles display a high extent of damage [26].

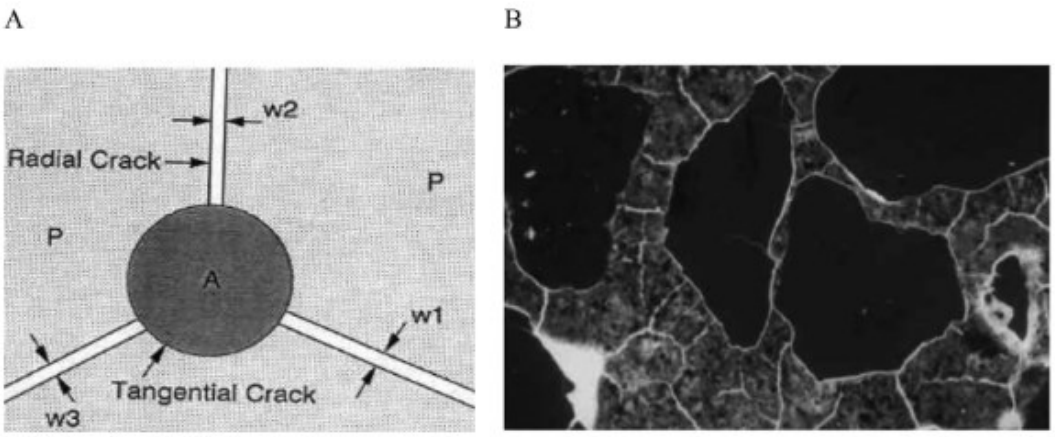

Figure 2.12 Shrinkage Distress Features: (A) Scheme with A Single Aggregate Particle And (B) Polished Concrete Surface [26]

Also, the phenomenon of shrinkage induces both radial and tangential strains in the cement paste and aggregates in Figure 2.12. Compressive stresses are frequently observed within the aggregate particles, while radial and tangential tensile stresses are formed in the bulk cement paste [26, 31]. Subsequent cracks develop when the magnitude of radial and tangential stresses surpass the material's tensile strength; in addition, it is important to note that shear stresses are also generated during this process, which might potentially result in the formation of shear cracks at ITZ [26]. Therefore, the distressed concrete affected by shrinkage manifests open radial cracks and thin shear cracks within the ITZ.

2.6 Research Gap

Although SEM, FEI with DIC and other related tools are powerful methods for high-resolution imaging and microanalysis, these tools present limitations. For example, SEM

can visually observe microcracks and chemical products, such as calcium silicate hydrate (CSH), within the hydrated cement paste and interfacial transition zone (ITZ), however, it lacks a systematic way of assessing the significance of the information conveyed by these images. Also, the algorithm designed for the DIC mentioned is unable to directly recognize the opening of a crack. Hence, DRI cannot only observe the crack pattern of drying shrinkage but is also a semi-quantitative approach for assessing the extent of damage caused by drying shrinkage in concrete. Therefore, in this research, DRI aims to effectively evaluate the crack in the microstructure of concrete according to the drying shrinkage level of the distinct exposure conditions.

2.7 References

[1] A. A. E. Elzokra, A. Al Houri, A. Habib, M. Habib, and A. Malkawi, "Shrinkage Behavior of Conventional and Nonconventional Concrete: A Review," Civ Eng J, vol. 6, no. 9, pp. 1839–1851, Sep. 2020, doi: 10.28991/cej-2020-03091586.

[2] P. K. Mehta and P. J. M. Monteiro, Concrete: microstructure, properties, and materials, 3rd ed. New York: McGraw-Hill, 2006.

[3] R. K. Mishra, R. K. Tripathi, and V. Dubey, "Early age shrinkage pattern of concrete on replacement of fine aggregate with industrial by-product," Journal of Radiation Research and Applied Sciences, vol. 9, no. 4, pp. 386–391, Oct. 2016, doi: 10.1016/j.jrras.2016.05.003.

[4] B. Bissonnette, P. Pierre, and M. Pigeon, "Influence of key parameters on drying shrinkage of cementitious materials," Cement and Concrete Research, vol. 29, no. 10, pp. 1655–1662, Oct. 1999, doi: 10.1016/S0008-8846(99)00156-8.

[5] A. M. Neville and J. J. Brooks, Concrete Technology, Second Edition.

[6] I. Maruyama, “Impact of drying on concrete and concrete structures,” RILEM Tech Lett, vol. 7, pp. 1–11, Jul. 2022, doi: 10.21809/rilemtechlett.2022.154.

[7] V. Gribniak, G. Kaklauskas, R. Kliukas, and R. Jakubovskis, “Shrinkage effect on short-term deformation behavior of reinforced concrete – When it should not be neglected,” Materials & Design, vol. 51, pp. 1060–1070, Oct. 2013, doi: 10.1016/j.matdes.2013.05.028.

[8] E. E. Holt and D. J. Janssen, “Influence of Early Age Volume Changes on Long-Term Concrete Shrinkage,” Transportation Research Record, vol. 1610, no. 1, pp. 28–32, Jan. 1998, doi: 10.3141/1610-05.

[9] C. De Sa, F. Benboudjema, M. Thiery, and J. Sicard, “Analysis of microcracking induced by differential drying shrinkage,” Cement and Concrete Composites, vol. 30, no. 10, pp. 947–956, Nov. 2008, doi: 10.1016/j.cemconcomp.2008.06.015.

[10] T. Akçaoğlu, M. Tokyay, and T. Çelik, “Assessing the ITZ microcracking via scanning electron microscope and its effect on the failure behavior of concrete,” Cement and Concrete Research, vol. 35, no. 2, pp. 358–363, Feb. 2005, doi: 10.1016/j.cemconres.2004.05.042.

[11] B. Al-Shathr, A. Abdulameer, and T. al-Attar, “The role of ambient temperature variation on drying shrinkage development of self-compacting Portland-limestone cement concrete,” MATEC Web Conf., vol. 162, p. 02021, 2018, doi: 10.1051/matecconf/201816202021.

[12] I. Maruyama, “Origin of Drying Shrinkage of Hardened Cement Paste: Hydration Pressure,” ACT, vol. 8, no. 2, pp. 187–200, Jun. 2010, doi: 10.3151/jact.8.187.

[13] H. Hyodo, R. Sato, K. Kawai, and H. Nakayama, "Effects of Drying Shrinkage on Shear Tension Strength of Reinforced Concrete Beams", in *8th International Conference on Fracture Mechanics of Concrete and Concrete Structures*, 2013.

[14] J. P. Ollivier, J. C. Maso, and B. Bourdette, “Interfacial Transition Zone in Concrete”.

[15] S. Jianxia, “Durability Design of Concrete Hydropower Structures,” in Comprehensive Renewable Energy, Elsevier, 2012, pp. 377–403. doi: 10.1016/B978-0-08-087872-0.00619-3.

[16] I. Adam, K. Sakata, and T. Ay, “Influence of Coarse Aggregate on the Shrinkage of Normal and High-Strength Concretes”.

[17] S. Nuhu, S. Ladan, and A. U. Muhammad, “Effects and Control of Chemical Composition of Clinker for Cement Production,” International Journal of Control Science and Engineering, vol. 10, no. 1, pp. 16–21, 2020, doi: 10.5923/j.control.20201001.03.

[18] J. Yang, Q. Wang, and Y. Zhou, “Influence of Curing Time on the Drying Shrinkage of Concretes with Different Binders and Water-to-Binder Ratios,” Advances in Materials Science and Engineering, vol. 2017, pp. 1–10, 2017, doi: 10.1155/2017/2695435.

[19] Y. Z. Yang, M. G. Li, H. W. Deng, and Q. Liu, “Effects of Temperature on Drying Shrinkage of Concrete,” AMM, vol. 584–586, pp. 1176–1181, Jul. 2014, doi: 10.4028/www.scientific.net/AMM.584-586.1176.

[20] F. Wittmann, Mechanisms and Mechanics of Shrinkage. 2001.

[21] F. H. Wittmann, “Shrinkage of High Strength Concrete as Compared to Shrinkage of Normal Strength Concrete - Significance for Crack Formation and Durability / Vergleichende Betrachtung des Schwindens von hoch festem und normalem Beton - Bedeutung für Rissbildung und Beständigkeit,” Restoration of Buildings and Monuments, vol. 10, no. 2, pp. 191–206, Apr. 2004, doi: 10.1515/rbm-2004-5846.

[22] A. Jenkins, “Implementation of ASTM C-157: Testing of Length Change of Hardened Concrete”.

[23] B. Suryanto, J. O. Buckman, P. Thompson, M. Bolbol, and W. J. McCarter, “Monitoring micro-crack healing in an engineered cementitious composite using the environmental scanning electron microscope,” Materials Characterization, vol. 119, pp. 175–185, Sep. 2016, doi: 10.1016/j.matchar.2016.07.021.

[24] Z. Ikhlasi, A. Gholampour, and T. Vincent, “Drying shrinkage of waste-based concrete reinforced with pristine graphene (PRG) nanomaterial,” Materials Today: Proceedings, p. S2214785323029176, May 2023, doi: 10.1016/j.matpr.2023.05.287.

[25] I. Maruyama and H. Sasano, “Strain and crack distribution in concrete during drying,” Mater Struct, vol. 47, no. 3, pp. 517–532, Mar. 2014, doi: 10.1617/s11527-013-0076-7.

[26] L. F. M. Sanchez, T. Drimalas, and B. Fournier, “Assessing condition of concrete affected by internal swelling reactions (ISR) through the Damage Rating Index (DRI),” Cement, vol. 1–2, p. 100001, Jun. 2020, doi: 10.1016/j.cement.2020.100001.

[27] L. F. M. Sanchez, T. Drimalas, B. Fournier, D. Mitchell, and J. Bastien, “Comprehensive damage assessment in concrete affected by different internal swelling reaction (ISR) mechanisms,” Cement and Concrete Research, vol. 107, pp. 284–303, May 2018, doi: 10.1016/j.cemconres.2018.02.017.

[28] L. F. M. Sanchez, B. Fournier, M. Jolin, D. Mitchell, and J. Bastien, “Overall assessment of Alkali-Aggregate Reaction (AAR) in concretes presenting different strengths and incorporating a wide range of reactive aggregate types and natures,” Cement and Concrete Research, vol. 93, pp. 17–31, Mar. 2017, doi: 10.1016/j.cemconres.2016.12.001.

[29] B. P. Gautam and D. K. Panesar, “The effect of elevated conditioning temperature on the ASR expansion, cracking and properties of reactive Spratt aggregate concrete,” Construction and Building Materials, vol. 140, pp. 310–320, Jun. 2017, doi: 10.1016/j.conbuildmat.2017.02.104.

[30] R.-P. Martin, L. Sanchez, B. Fournier, and F. Toutlemonde, “Evaluation of different techniques for the diagnosis & prognosis of Internal Swelling Reaction (ISR) mechanisms in concrete,” Construction and Building Materials, vol. 156, pp. 956–964, Dec. 2017, doi: 10.1016/j.conbuildmat.2017.09.047.

[31] A. Zahedi, C. Trottier, L. F. M. Sanchez, and M. Noël, “Microscopic assessment of ASR-affected concrete under confinement conditions,” Cement and Concrete Research, vol. 145, p. 106456, Jul. 2021, doi: 10.1016/j.cemconres.2021.106456.

3. Chapter Three: Assessment of Drying Shrinkage at Numerous Exposure Conditions

3.1 Abstract

Drying shrinkage in concrete is influenced by various ambient environmental conditions, including relative humidity and temperature. In this study, concrete specimens are fabricated in the laboratory to investigate the effects of numerous exposure conditions on the development of drying shrinkage over time. The specimens are maintained under varying conditions (i.e., 100%, 90%, 82%, 75%, 62% RH | 38 and 60 °C) to understand further the progression of drying shrinkage. These specimens were monitored within six months and assessed the mass and length change, and dynamic resonance frequency with the development of concrete maturity. Also, the porosity of concrete specimens stored at the high moisture conditions (i.e., 90%, 82%, and 75%) is closer to each. The findings demonstrate that concretes subjected to low relative humidity (i.e., 62%) exhibit the largest magnitude of drying shrinkage, most mass loss and highest porosity. However, the dynamic elastic modulus of the specimens does not appear to have a significant influence on drying shrinkage.

Keywords: Drying shrinkage, relative humidity, temperature, concrete maturity, elastic modulus, porosity.

3.2 Introduction

A significant effort has been made to improve concrete composition considering the current goal to reduce the concrete industry's contribution to CO_2 emission (ref). However, it is imperative to understand the distressing mechanisms with the potential to dimmish

concrete durability. The occurrence of cracking due to shrinkage in concrete is a significant issue, especially in the case of large infrastructure, such as bridges and highways, since it has the potential to facilitate degradation due to the ingress of other deleterious substances, triggering distressing mechanisms, such as corrosion [1-2]. Considering the advancing construction industry, it is crucial to possess a thorough effective assessment of the drying shrinkage phenomenon aiming to guarantee concrete durability.

Drying shrinkage is an essential consequence of moisture loss of concrete microstructure. This phenomenon involves a complex interaction between the molecular forces inside the material and the internal water movement within the pores network. The significance of this phenomenon lies in its ability to initiate fractures and distortions, ultimately posing a weakness to the structural integrity of concrete [3]. Therefore, it is important to understand the influence of environmental factors, such as relativity humidity and temperature levels regarding physical and mechanical properties. In this context, an experimental campaign was conducted aiming to assess the effect of drying shrinkage, triggered under distinct relative humidity and temperatures, on concrete properties. Laboratory samples were produced and stored under different environmental conditions monitoring physical and mechanical properties, such as mass and dimension changes, and porosity, as well as resonant responses, and dynamic modulus of elasticity, under distinct maturity levels. The standardized test on drying shrinkage mentioned in Section 2.4 was modified to consider the ASTM C1293 because this project was designed originally to evaluate drying shrinkage in ASR-affected concrete stored at low moisture conditions.

3.3 Background

3.3.1 Relative Humidity

The relative humidity plays a pivotal role in driving the phenomenon of drying shrinkage on concrete. Fluctuations in relative humidity can trigger either the absorption or desorption of moisture by the concrete [4]. These changes can lead to shifts in dimensions and internal strains, which can ultimately compromise the integrity of the concrete structure [7–11].

Concrete begins to lose water and undergo drying shrinkage when exposed to relative humidity levels lower than 100%. Capillary water within the concrete's micropores starts migrating and is gradually lost to the environment as the relative humidity drops below 100%. When the internal relative humidity of the concrete falls below 30%, the absorbed water is removed. Furthermore, when the relative humidity decreases to below 10%, interlayer water within the concrete structure also begins to be lost. Relative humidity also influences cement hydration since it is well established that sufficient moisture availability facilitates the chemical reaction between cement and water, forming hydration products that enhance the strength and durability of concrete [3]. Higher levels of relative humidity contribute to the prevention of untimely moisture loss, facilitating the continuous process of hydration and yielding an outcome of enhanced strength and resilience [4–6].

3.3.2 Temperature

Temperature is a significant role in the drying shrinkage of concrete. High temperatures can accelerate water evaporation, therefore, the loss of capillary water increases in the concrete to form larger drying shrinkage [3]. Meanwhile, since the temperature can accelerate the chemical reaction in the concrete, it increases the rate of water consumption

for the hydration reaction so that the internal relative humidity of the concrete decreases, therefore, the drying shrinkage is more prone to be induced on concrete. Furthermore, the hydration product is generated due to the accelerated hydration reaction by temperature in the early period, the rapid deformation of drying shrinkage on concrete is increased but the long-term deformation of concrete remains constant[12]. Also, it states that the rise in temperature can weaken the influence of the w/c ratio on the drying shrinkage of concrete[12].

3.3.3 Concrete Maturity

Although concrete is one of the most widely used construction materials, it is restricted and challenging to predict the time required to meet the required engineering properties. Concrete maturity is applied to estimate long-term concrete properties instead of time factor [13]. The maturity method uses the temperature history of the concrete to estimate the concrete's strength. The concept of concrete maturity was designed as a function of temperature and age that presents the mutual effect of time and temperature on concrete properties [14]. It states that the similar strengths of the identical mixtures are correlated with the same level of concrete maturity; therefore, it is also feasible to use non-destructive tools (NDT) to measure other concrete properties by monitoring temperature history [15]. Numerous researchers have proposed different maturity functions to explain the link between concrete temperature and time. Among these, the equivalent age function stands out as particularly recognized, as noted in ASTM C 1074 (ASTM 2017) [16] . This function is grounded in the Arrhenius equation, which illustrates the impact of temperature on the rate of chemical reactions, as highlighted by Freisleben Hansen and Pedersen (1977) [17].

$$M(t) = \sum(T_a - T_o)\,\Delta_t \quad (1)$$

where[16]:

$M(t)$: the temperature-time factor at age t, degree-days

Δ_t : a time interval, days

T_a : average concrete temperature during time interval Δ_t, ℃, and

T_o : datum temperature, ℃

3.4 Scope of Work

This study focuses on the influence of temperature and relative humidity on the behaviour of drying shrinkage; therefore, concrete specimens were fabricated using non-reactive aggregates in the laboratory and stored at different exposure conditions to enable the development of drying shrinkage and monitored over time. Also, the concept of concrete maturity is applied in the research to provide a comparison of the drying shrinkage behaviour between 38℃ and 60℃. These test methods applied are aimed to assess the performance of concrete undergoing drying shrinkage during a long term at the aspects of mass loss, length change of specimen, elastic modulus, and porosity.

3.5 Material of Methods

3.5.1 Materials, Mix Proportions and Exposure Conditions

A total of seventy-two, 100 mm by 200 mm, cylindrical concrete specimens were produced in the laboratory (i.e., 40 for each of the 38 ℃ group and 32 for the 60 ℃ group). The concrete mixture as shown in Table 3.1 was prepared with conventional GU cement, nonreactive coarse and fine aggregates. Hence, only drying shrinkage was considered. Also, Figure 3.1 illustrates that each moisture/temperature condition consists of 8 specimens with 2 buckets containing 4 specimens each.

Table 3.1 Mix Proportion of the Concrete Specimens

Ingredients	Weight (kg)	Specific Gravity
Cement	420.00	3.15
Coarse Aggregate	1002.45	2.79
Fine Aggregate	852.05	2.74

Figure 3.1 A Family under the same exposed condition

3.5.2 Fabrication

Cylindrical concrete specimens (100 mm diameter and 200 mm height) were cast instead of prims to facilitate further mechanical tests (e.g., shear and tension tests). After casting, the specimens were demolded and moist cured at room temperature for 48 hours; holes were drilled on both sides and studs were installed using a fast-setting cement slurry during the first 24 hours. The initial length readings were conducted after 48 hours, and specimens were ready for storage. Next, each family was set under different conditions according to different temperatures and relative humidity shown in Table 3.2; thereby inducing the drying shrinkage and monitoring over time.

Table 3.2 The Different Exposure Conditions

Temp (°C)/RH (%)	**100**	**90**	**82**	**75**	**62**
38	100%-38°C	90%-38°C	82%-38°C	75%-38°C	62%-38°C
60		90%-60°C	82%-60°C	75%-60°C	62%-60°C

3.5.3 Control and measurement of Relative humidity

One of the widespread methods for controlling relative humidity and temperature for experiments requiring a controlled environment is the use of environmental chambers, which are expensive and could also delay other experimental works. Its use becomes more complicated given the number of samples and different moisture conditions needed for this research. As a result, the traditional method of controlling RH with the aid of saturated salt solutions, as described in ASTM E104 [16], was adopted. Table 3.3 shows all the salt solutions used to achieve all the moisture and temperature combinations.

Table 3.3 Salt solution and RH conditions

Temp/RH	**62%**	**75%**	**82%**	**90%**	**100%**
38°C	sodium nitrite	sodium chloride	potassium chloride	potassium nitrate	distilled water
60°C	sodium nitrite	sodium chloride	potassium nitrate	potassium sulfate	

Water/saturated salt solution is placed in the bottom of each container for all conditions as highlighted in Table 3.3 and concrete specimens were stored on a perforated rack above the water/saturated salt solution. The relative humidity in each container was monitored

over time with the aid of ibutton sensors, which was selected for this study due to their ability to function and save data independently without needing a data logger.

3.5.3 Drying Shrinkage Measurement

The length change of the specimen was measured for six months using the apparatus shown in Figure 3.2 which has been widely used by several studies to assess length change in concrete undergoing internal swelling reactions [15–17]. The initial length of the specimens was measured 48 hours after the fabrication. Then, the measurement was done biweekly; meanwhile, the bottom of each specimen was always inverted to ensure uniform moisture exposure and to minimize the impact of moisture gradients occurring in the specimen. The collected data is subsequently graphed and subjected to analysis to identify patterns and establish correlations between the length change and the distinct relative humidity.

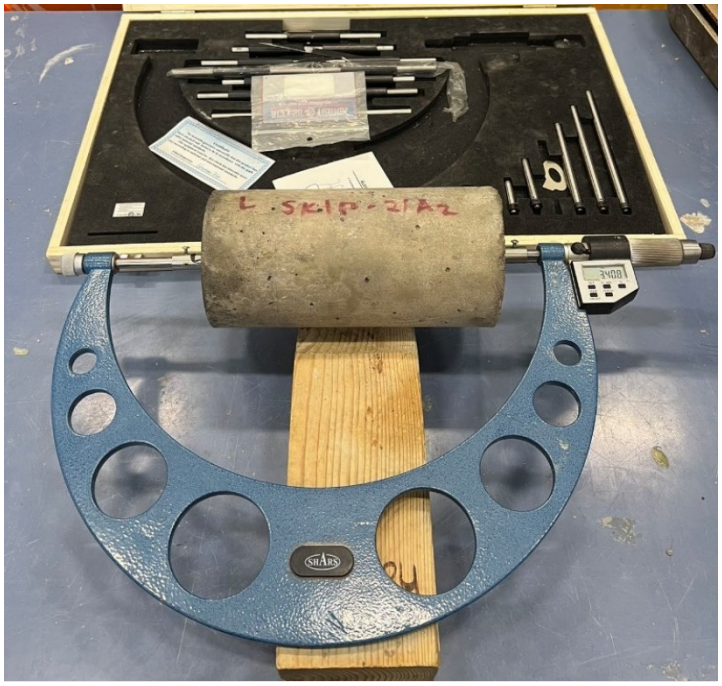

Figure 3.2 Length Change Measurement

3.5.4 Dynamic Resonance Frequency Test

Resonance frequency refers to the frequency at which a material naturally vibrates or resonates when subjected to an external force; meanwhile, it is often associated with non-destructive testing (NDT) of concrete materials. According to ASTM C 215-19 [20], the transverse mode of impact resonance method is applied to determine the resonance frequency, which is subsequently utilized in the calculation of the dynamic Young's modulus of elasticity. In this project, this test is applied on the same day as the length and mass change measurement; thus, the dynamic elastic modulus corresponds to the specimen's length change and mass loss.

3.5.5 Mass Measurement

The measurement of mass in concrete specimens over time is shown in Figure 3.3. It is an essential process for understanding the phenomena of drying shrinkage and the overall durability of concrete. In this work, this test was conducted periodically for 6 months. Also, the initial mass measurement was on the 7^{th} day after batching and the successive measurement took place on the same day with drying shrinkage measurements and dynamic resonance frequency test. The comparison of these successive measurements with the original masses of the specimens determined the percentage of loss in mass. The test aims to establish a function with time and mass loss so that it assesses the deterioration of drying shrinkage on the concrete.

Figure 3.3 Mass Measurement

3.5.6 Porosity Test

Porosity refers to the extent of empty spaces present within the concrete matrix, and it is important in determining the concrete's capacity to withstand moisture penetration, chemical deterioration, and structural degradation over its lifespan. In this project, each specimen was cut into three parts (top, middle and bottom shown in Figure 3.4) at the end of the length and mass change measurements. Thereafter, the specimens were oven-dried to constant mass. Thereafter, the dried specimens were submerged in a vacuum container filled with water, ensuring that the water level exceeded the top surface of all specimens. The pump was then activated until it reached a pressure of 29 inHg and left running for a duration of 3 to 5 minutes. Subsequently, the specimens were maintained under vacuum conditions for 24 hours. Finally, after 24 hours, the specimens were removed from the vacuum container and their surfaces were dried using a cloth to measure saturated surface dry mass (Mssd). The final procedure was determining the submerged mass, utilizing

Archimedes' principle, by submerging the mass in the coarse aggregate basket immediately after the measurement of Mssd.

Figure 3.4 Porosity Test: Cutting the Specimen into three parts:(Top, Middle, Bottom), Vacuum Container and Submerged Mass Measurement Table

3.6 Results

3.6.1 Development of Drying Shrinkage

The main objective of this study is to investigate the impact of different exposure conditions on drying shrinkage specimens. Meanwhile, the concept of concrete maturity is applied, which integrates temperature and time to evaluate the long-term and short-term behaviour of the concrete specimen, therefore, it is compared for the drying shrinkage of concrete with identical relative humidity at different temperatures. As shown in Figure 3.5 (a) and (b) it presents the average of the length change experienced by 8 concrete specimens for each moisture condition.

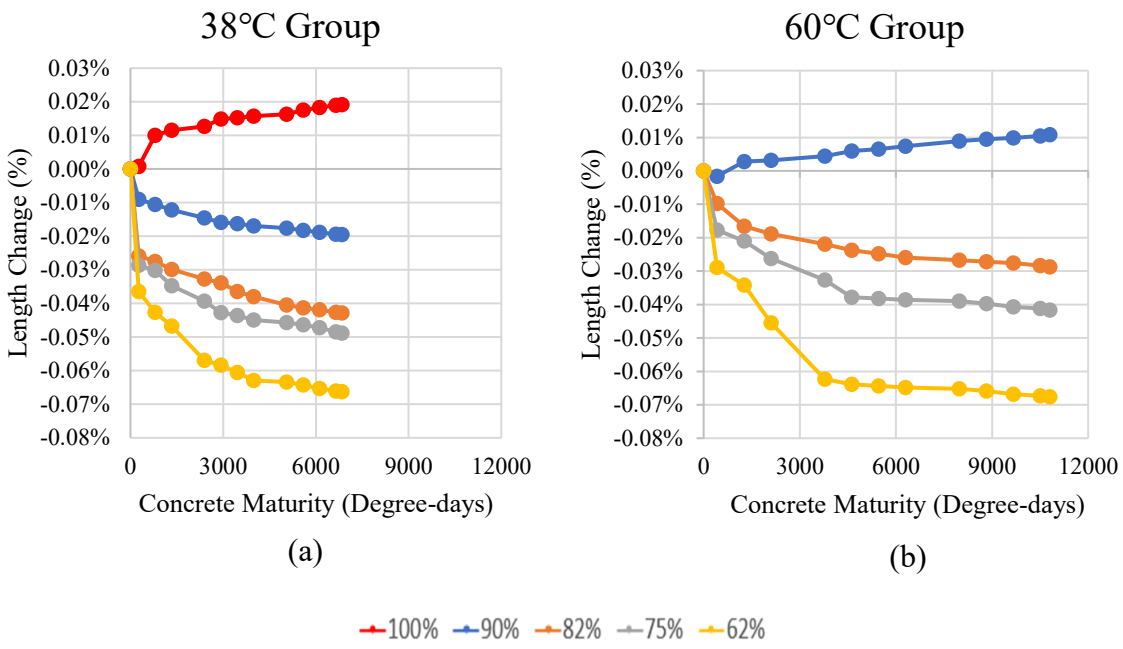

Figure 3.5 Length Change According to the Concrete Maturity (Degree-days)

Firstly, in Figure 3.5, these specimens stored at exposure conditions of 100% RH at 38℃ and 90% RH at 60℃ attained an expansion during the experiment. This expansion is observed despite the non-reactivity of the aggregates. The expansion is within the stated limits of the permitted expansion, as specified by CSA A23.2-27A, for non-reactive aggregate (i.e., < 0.040% at one year). Also, the length change of the specimen of RH 90% with 60℃ shrunk at the concrete maturity of 420 degree days and then expanded until the end. It explains that the concrete, in this case, underwent initial drying shrinkage because of water loss under the relative humidity of 90%; but then, it depicted expansion at a later age.

In the case of the 38℃ group, Figure 3.5 (a) shows the specimens with different relative humidity (i.e., 90%, 82%, 75%, 62%) reached the maximum drying shrinkage level (i.e., -0.0195%, -0.0428%, -0.0488%, -0.00663%) at the concrete maturity of 6480 degree-days. Also, the specimen with the saturated condition (100%) experienced an expansion of

0.0191%. In the case of the 60℃ group, all specimens attained longer concrete maturity because of the high temperature as Figure 3.5 (b) shows. The specimens with different relative humidity (i.e., 82%, 75%, 62%) reached the maximum drying shrinkage level (i.e., -0.0287%, -0.0416%, -0.0676%) at the concrete maturity of 10800 degree-hours, while the specimens stored at 90% RH attained an expansion of 0.0108%.

The influence of relative humidity at 38℃ and 60℃ conditions was illustrated in Figure 3.6. At the early maturity (0-1000 Degrees), the rate of drying shrinkage of the 38℃ group is faster than the 60 ℃ group. Moreover, the specimens in the 60℃ group present a higher length change (e.g., 90%, 82% and 75% RH) compared with the 38℃ group within 7000-degree days. Also, the specimens with 90% RH in 60℃ had already shown expansion when the concrete maturity reached 798 degree-days. Considering the 62% RH condition, although the specimen stored in 62% RH-60℃ underwent less drying shrinkage than those in 62%RH-38℃, nevertheless, both specimens attained similar shrinkage levels (-0.0627%, and -0.0629%) at the concrete maturity of 3990 degree-days.

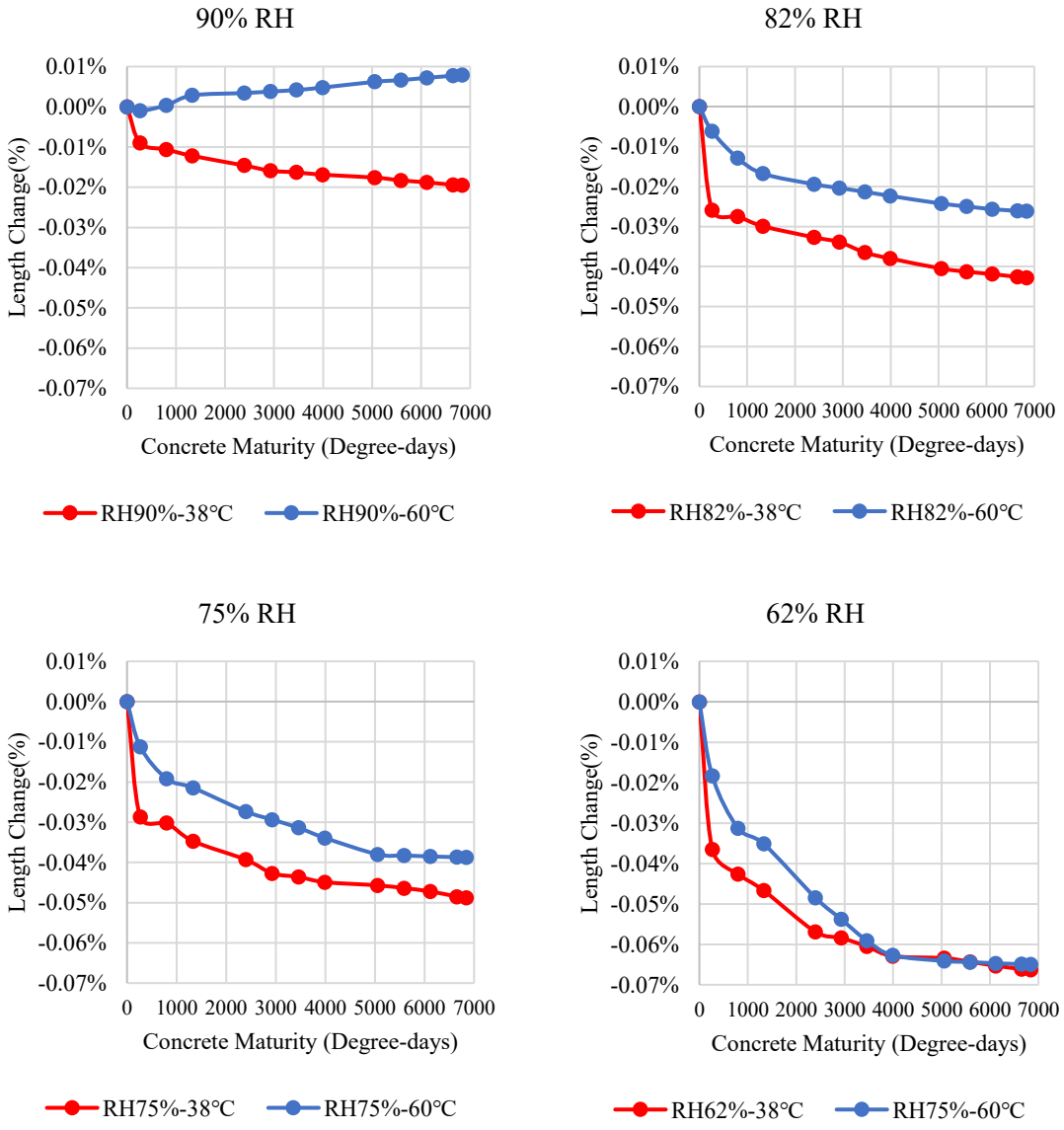

Figure 3.6 The Comparison of Distinct Relative Humidity between the 38°C Group and 60°C Group with A Range of the Same Concrete Maturity

Figure 3.7 illustrates the mass change that occurred at different exposure conditions. The mass change of concrete during drying shrinkage is influenced by two major factors: the degree of hydration, which impacts the amount of CSH products formed by the hydration reaction, and the moisture content, which is influenced by water evaporation caused by drying shrinkage.

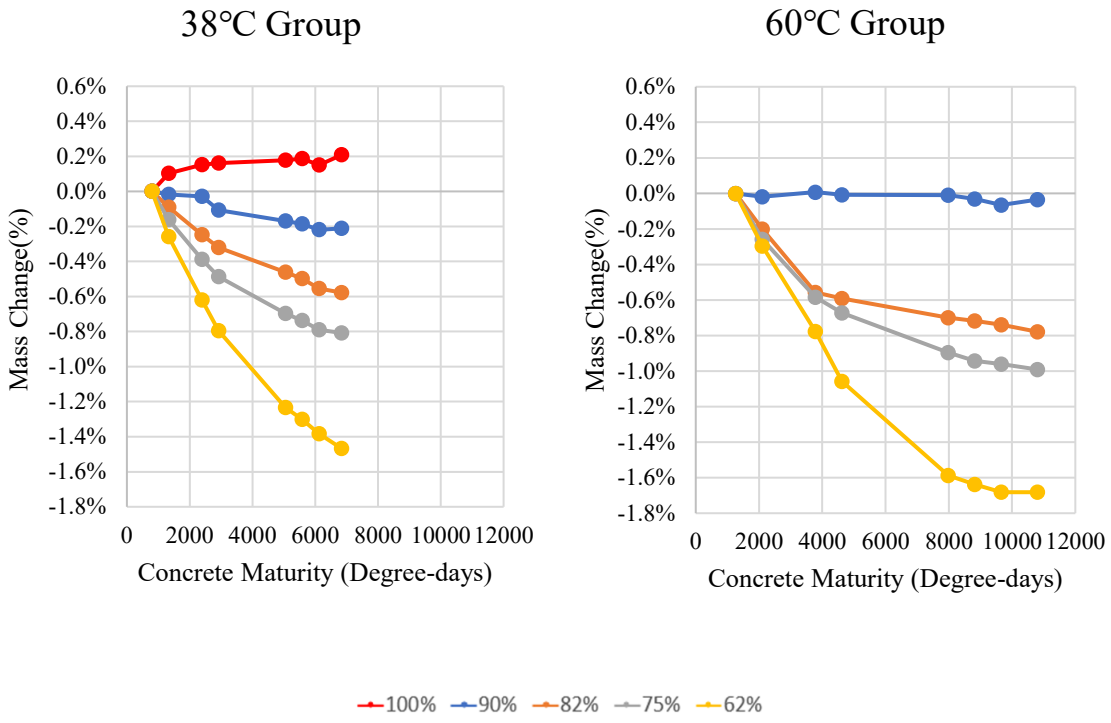

Figure 3.7 The Mass Change of the 38℃ Group and 60℃ Group

In the 38℃ group, the case of 100% RH presents an increase in mass because no water loss occurs and the hydration reaction continues to generate CSH, which enhances the strength of the concrete, as shown by the increase of concrete maturity; meanwhile, the case of the other four exposure conditions (90%, 82%, 75%, 62% RH) measured the distinct extent of mass loss (-0.212%, -0.557%, -0.808%, -1.467%) at the final concrete maturity of 5040 degree-days. In the 60℃ group, all specimens under the different exposure conditions (i.e., 90%, 82%, 75%, 62% RH) attained the mass loss (i.e., -0.035%, -0.779%, -0.991%, and -1.682%) after 180 days (10800 degree-days).

3.6.2 Influence of Drying Shrinkage on Porosity

The porosity results for specimens stored at different exposure conditions are illustrated in Figure 3.8. Among the samples in the 38℃ group, it is seen that the sample with a relative humidity of 62% exhibits a maximum porosity of 11.15%, while the sample with a RH of 100% has the lowest porosity of 7.87%. Also, the porosity values of relative humidity of 90%, 82%, and 75% exhibit a decrease, specifically to 9.79%, 9.36%, and 9.22% respectively. In the 60℃ group, the specimens with a relative humidity of 62% present the highest porosity of 12.37%; meanwhile, the difference in the porosity of these specimens with the relative humidity of 90% and 82% are small (8.31% and 8.12%).

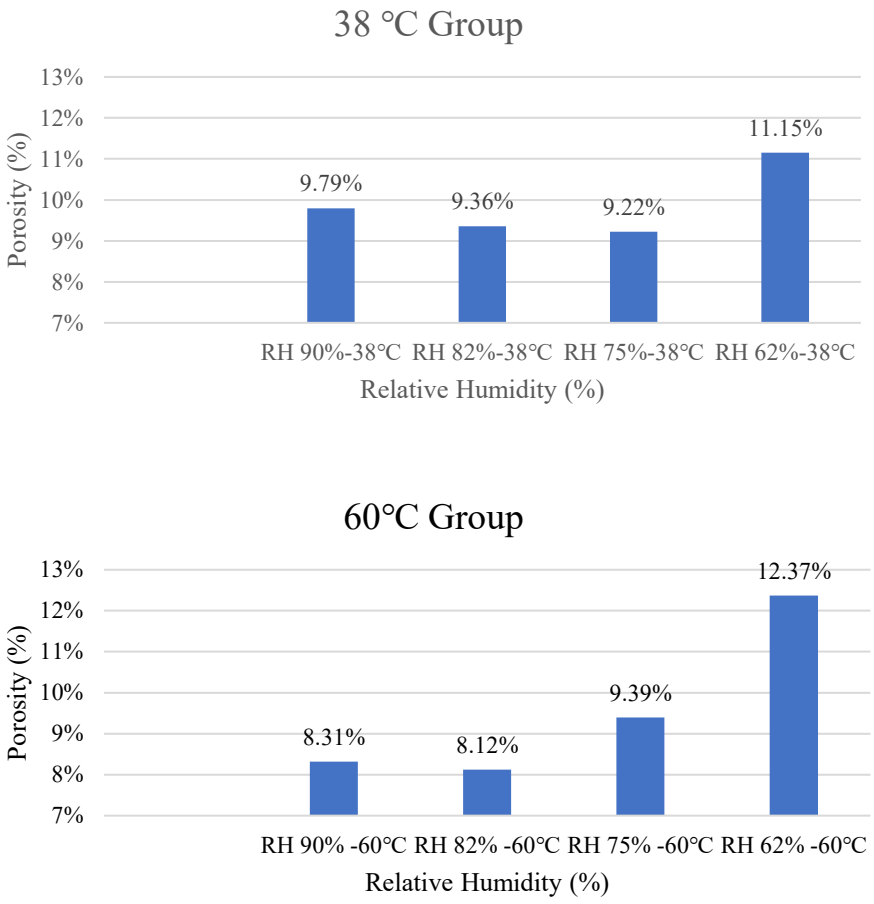

Figure 3.8 The Influence of Temperature and Relative Humidity on Porosity

3.6.3 Dynamic Modulus of Elasticity and Drying Shrinkage

Figure 3.9 illustrates the change in the dynamic elastic modulus of specimens under distinct exposure conditions. As shown in the results, the specimens with higher relative humidity obtained a higher elastic modulus throughout the entire project.

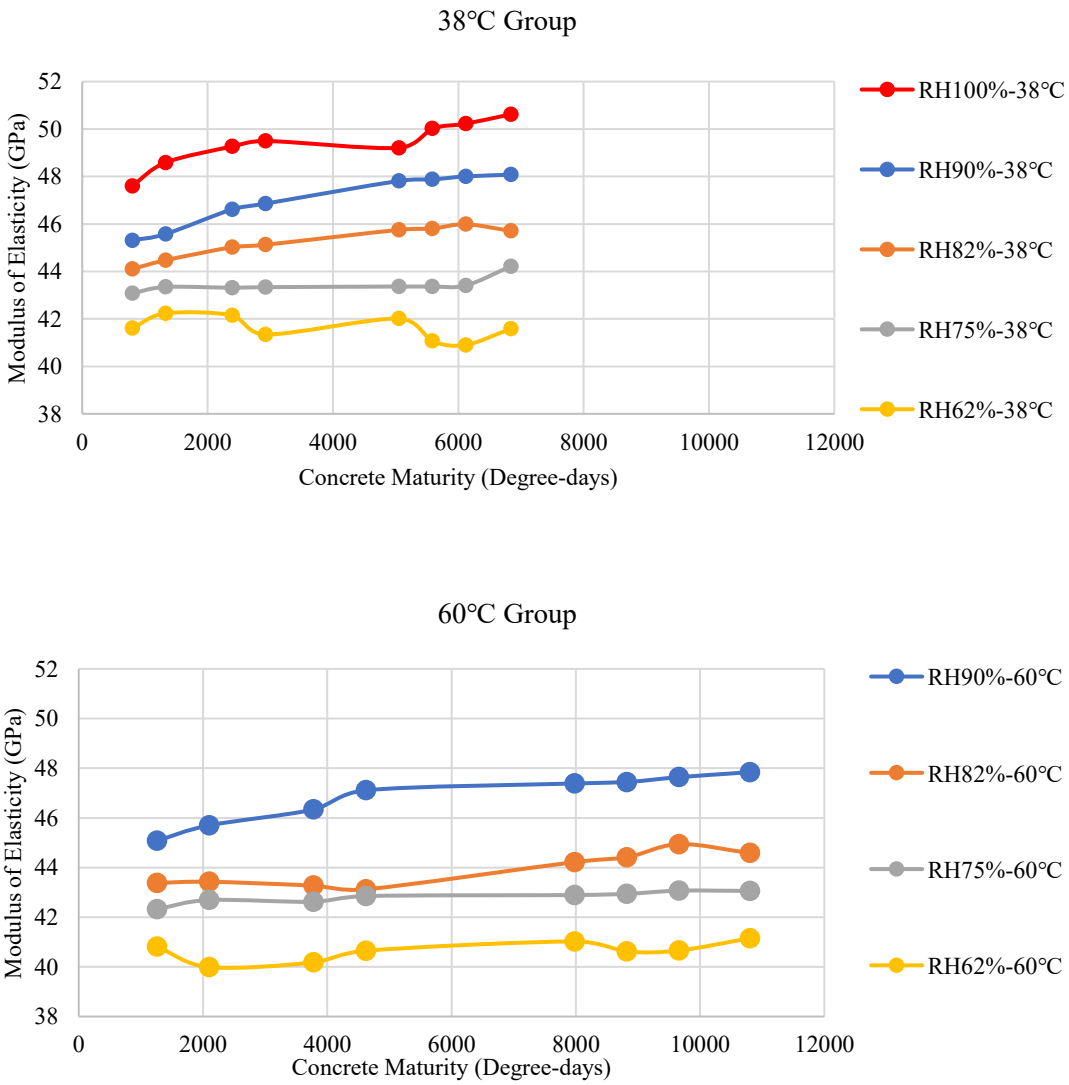

Figure 3.9 Dynamic Elastic Modulus vs. Concrete Maturity

The dynamic elastic modulus of specimens in the 38°C group was measured under various relative humidity levels of 100%, 90%, 82%, 75%, and 62%. The initial measurements, taken at a concrete maturity of 798-degree days, obtained values of 47.61GPa, 45.31GPa,

44.10GPa, 43.08GPa, and 41.61GPa, respectively. After 180 days, the dynamic elastic modulus for each exposure condition changed to 50.63GPa, 48.08GPa, 45.71GPa, 44.22GPa, and 41.59GPa. Particularly, the dynamic elastic modulus experiences an increase when compared to the original value for all relative humidity levels, with percentage increases of 6.3%, 6.1%, 3.6%, and 2.6%. However, it is worth noting that the relative humidity of 62% exhibits a minor decrease in the elastic modulus, with a decrease of -0.05%.

In the other case of 60℃, at the beginning with the concrete maturity of 1260 degree days, the elastic modulus of the specimens is measured as 45.08GPa, 43.38GPa, 42.33GPa, and 40.82GPa according to the different relative humidity levels of 90%, 82%, 75%, and 62%. After 180 days, the concrete maturity reaches 10800-degree days while the modulus of elasticity increases to 47.84GPa, 44.59GPa, 43.06GPa, and 41.15GPa. The total elastic modulus experiences a percentage change of 6.1%, 2.8%, 1.7%, and 0.8% for relative humidity levels of 90%, 82%, 75%, and 62%, respectively.

3.7 Discussions

3.7.1 Development of Drying Shrinkage at Numerous Relative Humidity and Temperature

Figure 3.5 and Figure 3.7 illustrate the length and mass change of concrete specimens stored at numerous exposure conditions. Firstly, a reduction in the relative humidity induces a high level of drying shrinkage. Also, it is observed that the drying shrinkage (for 90%, 82%, and 75% RH) at the end of the concrete maturity of 38℃, which is approaching 7000 degree-days, is close to the amount observed at half of the concrete maturity of the 60℃ group. Therefore, comparing the 38℃ group with the 60℃ group at the identical concrete maturity range (i.e., 0-6840 degree-days) shown in Figure 3.6, the length changes

(especially the drying shrinkage) for all exposure conditions in the 60℃ group are lower than 38℃ group. In other terms, the final drying shrinkage values for the groups exposed to a temperature of 38℃ are 0.0195%, -0.0428%, -0.0488%, and -0.0663% for relative humidity levels of 90%, 82%, and 75% respectively, after 180 days. Similarly, the final drying shrinkage values for the groups exposed to a temperature of 60℃ are 0.0079%, -0.0262%, -0.0387%, and -0.0649% for relative humidity levels of 90%, 82%, 75% and 62% respectively, after 114 days. Therefore, it can be found that the concrete specimens with identical relative humidity under a higher temperature environment over a shorter duration are comparatively smaller in magnitude when compared to the drying shrinkage under a lower temperature environment over a longer duration, even though the concrete maturity can be the same.

Figure 3.5 shows the multiple phases on the rate of length change found in both 38℃ and 60℃ groups. In the case of 38℃ groups, it exhibits three phases of length change for the lower moisture conditions (i.e., RH of 90%, 82%,75%,62%). Specifically, the length change of specimens experiences a rapid drop during the initial phase (0-266 degree-days); then, it contains a moderate decrease when the concrete maturity range is between 266 and 2926 degree-days followed by a stable slight decline toward the final phase (2926-6840 degree-days). Similarly, it is observed that specimens subjected to temperatures of 60℃ exhibit three phases of length change for the lower moisture conditions (i.e., RH of 82%,75%,62%). Specifically, these specimens experience a drop during the initial phase (0-420 degree-days) and then a moderate decline (420-4620 degree-days) followed by a stable slight decline towards the final phase (4620-10800 degree-days). It states that although the concrete maturity of the specimens under the different exposure conditions is

different, the three phases with different rate of length change due to drying shrinkage is essential; meanwhile, the rate of length change is correlated to the extent of relative humidity. The decrease in relative humidity leads to a more pronounced increase in the rate of length change during the first two phases.

Figure 3.7 illustrates that concrete specimens demonstrated a more pronounced decrease in mass when exposed to an environment characterized by low relative humidity. The specimens that were subjected to relative humidity (RH) of 62% demonstrate the most significant magnitude of mass loss. In contrast, the specimens exposed to a relative humidity (RH) of 90% undergo a small rate and extent of mass reduction. Additionally, it is observed that the specimens stored at a relative humidity (RH) of 75% exhibit a slightly higher mass loss compared to those conditioned at 82% RH. Additionally, it is seen that specimens with a higher degree of concrete maturity (ranging from 1260 to 10800-degree days) demonstrate the most significant final mass loss. Conversely, specimens with a lower degree of concrete maturity (ranging from 798 to 5040-degree days) indicate the largest rate of mass loss. It means that concrete loses more mass at high concrete maturity, but the concrete will lose mass quickly at low concrete maturity. Hence, it can be inferred that a low degree of hydration could occur at low concrete maturity and relative humidity. Therefore, the hydration reaction does not have sufficient water to generate CSH and other products in the concrete while the water evaporation is caused by drying shrinkage on concrete.

3.7.2 Influence of Drying Shrinkage on Elastic Modulus

In this work, the dynamic modulus of elasticity is measured by the dynamic resonance frequency to assess the stiffness of concrete specimens and their capacity to undergo

deformation under the influence of tensile stress caused by drying shrinkage. Figure 3.9 indicates a decrease in the elastic modulus of concrete when subjected to low relative humidity conditions because the specimen with low relative humidity causes increased permeability as a result of a greater number of cracks in the cement paste and decreased strength due to insufficient water for the continuation of the hydration reaction [3] so that the low relative humidity contributes to decreased stiffness compared to high relative humidity conditions. Also, a tendency was observed towards greater values of the dynamic elastic modulus as the maturity of the concrete increases.

However, the variation rate of dynamic elastic modulus for all specimens is not as distinct as that of length and mass shown in Figure 3.5 and Figure 3.7. When subjected to the same relative humidity, the specimens in both temperature groups provide similar data on the dynamic elastic modulus, regardless of whether the measurements were taken initially or at the end. It can be explained by restraint from aggregate components on dynamic elastic modulus. Nevertheless, the dynamic elastic modulus still depicted minor changes reflected by the drying shrinkage. At the concrete maturity of 6840 degree-days, the dynamic elastic modulus of the 38°C group obtained percentage change of 6.1%, 3.6%, 2.6%, and -0.05%. At the concrete maturity of 10800 degree-days, the dynamic elastic modulus of the 60°C group obtained a percentage change of 6.1%, 2.8%, 1.7%, and 0.8% for relative humidity levels of 90%, 82%, 75%, and 62%, respectively. Based on the findings, the change in dynamic elastic modulus of the specimen with low relative humidity is small compared to that of high relative humidity. The specimen with low relative humidity does not save sufficient water for the continuation of the hydration reaction; thus, the change in the dynamic elastic modulus becomes smaller for a long term of 180 days.

3.7.3 Porosity of drying shrinkage specimens

It was observed that the porosity of concrete specimens with high relative humidity (i.e., 90%,82% and 75% in the 38°C group and 90% and 82% in the 60°C group) is determined within a range (9.79%, 9.36%, and 9.22% in the 38°C group; 8.31% and 8.12% in the 60°C group) (Figure 3.8). In this case, these concrete specimens are effectively keeping a substantial quantity of moisture to reduce the water consumption due to both drying shrinkage and hydration reaction; also, it indicates the presence of water fills up the voids inside the concrete. A decrease in porosity often confers advantageous effects on the strength and durability of concrete. Meanwhile, a decrease in relative humidity (e.g., 62%) results in reduced moisture content within the concrete specimen, potentially increasing porosity. The loss of moisture can result in the amplification of voids inside the concrete, which has the potential to cause an increase in porosity levels. In addition, if a concrete mixture has higher porosity, it may have more interconnected voids, allowing water to evaporate more easily. The consequence of this phenomenon is not only an increase in dry shrinkage due to the evaporation of moisture from the empty spaces but also an enhancement in the permeability of these specimens. Moreover, the existence of voids might facilitate the occurrence of shrinkage, hence increasing the likelihood of crack formation. Therefore, an inverse relationship is manifested between relative humidity and porosity, whereby higher relative humidity levels are correlated with decreased porosity and potentially reduced dry shrinkage. Conversely, lower humidity levels can result in increased porosity and potential vulnerability to dry shrinkage-related problems such as cracking.

3.7 Conclusion

This study aimed to understand the influence of drying shrinkage on the physical and mechanical properties of the concrete specimen stored at different exposure conditions. The main findings of this chapter are presented below:

- Low moisture condition causes severe drying shrinkage in concrete. Meanwhile, the concrete stored at low temperatures generates a larger length change at high moisture conditions (such as 90%, 82%, and 75%). However, at the same concrete maturity, the concrete specimens with identical relative humidity under a higher temperature environment (60℃) over a shorter duration are comparatively smaller in magnitude when compared to the drying shrinkage under a lower temperature environment (38℃) over a longer duration. Significantly, the extent of mass loss from concrete is significantly higher compared to that of dry shrinkage. Consequently, even a minimal quantity of dry shrinkage leads to a considerable reduction in the mass of the concrete. Moreover, as concrete maturity increases, the extent of drying shrinkage and mass loss becomes increasingly pronounced. Also, under identical concrete maturity, the change of mass and length induced by drying shrinkage on concrete developed rapidly in the first few weeks (21 days after batching); however, it is observed that these changes perform a gradual and slight decline for the final 100 days.
- The drying shrinkage behaviour only slightly affects the development of the elastic modulus of concrete because this property is mainly influenced by the coarse aggregate. Thus, it is essential to apply other methods to evaluate the drying

shrinkage behaviour on the concrete matrix, since the drying shrinkage occurs and causes damage to the hydrated cement paste.

- An inverse relationship is manifested between relative humidity and porosity, whereby higher relative humidity levels are correlated with decreased porosity and potential mitigation of dry shrinkage. Conversely, lower humidity levels can result in increased porosity and an increased vulnerability to dry shrinkage-related problems such as cracking.

3.8 Reference

[1] R. Ramírez, E. L. Chagoyén, and J. F. Martirena, 'Assessment of factors influencing the development of drying shrinkage in concretes produced in Cuba', *Obras y Proyectos*, no. 26, pp. 100–112, Dec. 2019, doi: 10.4067/S0718-28132019000200100.

[2] K. Folliard, 'Evaluation of Alternative Materials to Control Drying-Shrinkage Cracking in Concrete Bridge Decks'.

[3] P. K. Mehta and P. J. M. Monteiro, *Concrete: microstructure, properties, and materials*, 3rd ed. New York: McGraw-Hill, 2006.

[4] I. Maruyama, 'Origin of Drying Shrinkage of Hardened Cement Paste: Hydration Pressure', *ACT*, vol. 8, no. 2, pp. 187–200, Jun. 2010, doi: 10.3151/jact.8.187.

[5] F. H. Wittmann, 'Shrinkage of High Strength Concrete as Compared to Shrinkage of Normal Strength Concrete - Significance for Crack Formation and Durability / Vergleichende Betrachtung des Schwindens von hoch festem und normalem Beton - Bedeutung für Rissbildung und Beständigkeit', *Restoration of Buildings and Monuments*, vol. 10, no. 2, pp. 191–206, Apr. 2004, doi: 10.1515/rbm-2004-5846.

[6] I. Maruyama, ‘Impact of drying on concrete and concrete structures’, *RILEM Tech Lett*, vol. 7, pp. 1–11, Jul. 2022, doi: 10.21809/rilemtechlett.2022.154.

[7] I. Yoshida, H. Kanemitsu, M. Yamashita, and K. Higuchi, ‘Seismic Analysis of R. C. Pier with Earthquake Resistant Wall’, *Doboku Gakkai Ronbunshu*, vol. 1987, no. 386, pp. 349–358, Oct. 1987, doi: 10.2208/jscej.1987.386_349.

[8] Frank J. Vecchio and Michael P. Collins, ‘The Modified Compression-Field Theory for Reinforced Concrete Elements Subjected to Shear’, *ACI Journal Proceedings*, vol. 83, no. 2, Jan. 1986, doi: 10.14359/10416.

[9] H. Hyodo, R. Sato, K. Kawai, and H. Nakayama, ‘Effects of Drying Shrinkage on Shear Tension Strength of Reinforced Concrete Beams’.

[10] B. Bissonnette, P. Pierre, and M. Pigeon, ‘Influence of key parameters on drying shrinkage of cementitious materials’, *Cement and Concrete Research*, vol. 29, no. 10, pp. 1655–1662, Oct. 1999, doi: 10.1016/S0008-8846(99)00156-8.

[11] J. Kinda *et al.*, ‘Investigation of microscopic creep and shrinkage deformations of cement paste assisted by digital image correlation technique’, *Cement and Concrete Research*, vol. 166, p. 107101, Apr. 2023, doi: 10.1016/j.cemconres.2023.107101.

[12] Y. Z. Yang, M. G. Li, H. W. Deng, and Q. Liu, ‘Effects of Temperature on Drying Shrinkage of Concrete’, *AMM*, vol. 584–586, pp. 1176–1181, Jul. 2014, doi: 10.4028/www.scientific.net/AMM.584-586.1176.

[13] D. Miller, N.-M. Ho, and N. Talebian, ‘Monitoring of in-place strength in concrete structures using maturity method – An overview’, *Structures*, vol. 44, pp. 1081–1104, Oct. 2022, doi: 10.1016/j.istruc.2022.08.077.

[14] A. G. A. Saul, ‘Principles underlying the steam curing of concrete at atmospheric pressure’, *Magazine of Concrete Research*, vol. 2, no. 6, pp. 127–140, Mar. 1951, doi: 10.1680/macr.1951.2.6.127.

[15] G. Kampli, S. Chickerur, and M. V. Chitawadagi, ‘Real-time in-situ strength monitoring of concrete using maturity method of strength prediction via IoT’, *Materials Today: Proceedings*, vol. 88, pp. 110–118, 2023, doi: 10.1016/j.matpr.2023.05.610.

[16] ‘ASTM C 1074 Standard Practice for Estimating Concrete Strength by the Maturity Method’, 2017.

[17] P. F. Hansen and E. J. Pedersen, ‘Maturity computer for controlled curing and hardening of concrete’, Nordiska Betongfoerbundet, 1977.

[18] D22 Committee, ‘Practice for Maintaining Constant Relative Humidity by Means of Aqueous Solutions’, ASTM International. doi: 10.1520/E0104-20A.

[19] R.-P. Martin, L. Sanchez, B. Fournier, and F. Toutlemonde, ‘Evaluation of different techniques for the diagnosis & prognosis of Internal Swelling Reaction (ISR) mechanisms in concrete’, *Construction and Building Materials*, vol. 156, pp. 956–964, Dec. 2017, doi: 10.1016/j.conbuildmat.2017.09.047.

[20] A. Zahedi, C. Trottier, L. F. M. Sanchez, and M. Noël, ‘Microscopic assessment of ASR-affected concrete under confinement conditions’, *Cement and Concrete Research*, vol. 145, p. 106456, Jul. 2021, doi: 10.1016/j.cemconres.2021.106456.

[21] L. F. M. Sanchez, T. Drimalas, B. Fournier, D. Mitchell, and J. Bastien, ‘Comprehensive damage assessment in concrete affected by different internal

swelling reaction (ISR) mechanisms', *Cement and Concrete Research*, vol. 107, pp. 284–303, May 2018, doi: 10.1016/j.cemconres.2018.02.017.

[22] C09 Committee, 'Test Method for Fundamental Transverse, Longitudinal, and Torsional Resonant Frequencies of Concrete Specimens', ASTM International. doi: 10.1520/C0215-19.

4. Chapter Four: Microscopic Assessment of Drying Shrinkage induced Deterioration.

4.1 Abstract

Assessing concrete integrity involves understanding shrinkage-induced microstructure changes, which can lead to cracks, altering affected concrete properties. In this study, concrete specimens are stored at five distinct relative humidity (100%, 90%, 82%,75%, and 62%) and two temperatures (38℃ and 60℃). The damage rating index (DRI) has previously proven successful and widely used in the microscopic assessment of the internal swelling reaction mechanism in concrete, this study aims to utilize the DRI to evaluate the influence of damage caused by drying shrinkage on concrete at numerous moisture conditions. Significantly, it states the increase in the number of cracks induced by drying shrinkage, which are mainly the cracks in the cement paste (CCP) that occur at the concrete specimen stored at low moisture conditions (i.e., 62%). Meanwhile, the DRI value performs an increasing trend according to the larger drying shrinkage with a decrease in the relative humidity of concrete.

Keywords: Drying shrinkage, damage rating index (DRI), relative humidity, cracks in the cement paste (CCP), microscopic assessment

4.2 Introduction

The phenomenon of drying shrinkage in concrete has been well recognized as a significant factor impacting the durability and integrity of buildings and infrastructure. As the moisture content of concrete decreases, it undergoes a process of drying shrinkage, which subsequently gives rise to a variety of issues including cracking, diminishing structural integrity, and increasing permeability. Although traditional approaches to evaluating

drying shrinkage have provided significant insights, the development of advanced microscopic techniques holds the potential for thorough assessments of damaged concrete. DRI has been proven effective in assessing internal swelling reaction (ISR) mechanisms, such as alkali-silica reaction (ASR), delayed ettringite formation (DEF) and freezing and thawing cycles (FT) [1–3]. Shrinkage damage signs have similarities with those from ISR mechanisms, it initiates fractures and distortions in the material microphases, ultimately posing a weakness to the structural integrity of concrete [4]. Understanding shrinkage-affected concrete requires analyzing microfeatures impacted by environmental factors, such as humidity and temperature using powerful microscopic tools. In this context, an experimental campaign was conducted to assess the impact of drying shrinkage, developed under varying relative humidity and temperature conditions, on concrete microstructure. Laboratory samples were produced and stored under different environmental conditions. The dimension changes were monitored over time, and damage signs and patterns were assessed through DRI.

4.3 Scope of Work

This study aims to assess the efficiency of the damage rating index to quantitatively evaluate the deterioration of drying shrinkage on concrete at distinct moisture and temperature conditions. The deterioration induced by drying shrinkage presents cracks in the concrete base on the different levels of drying shrinkage. All concrete specimens are made of non-reactive materials and stored at five different relative humidity (100%, 90%, 82%, 75%, and 62%) and temperatures (i.e., 38℃ and 60 ℃). Firstly, it is going to observe crack patterns and account for the cracks in the drying shrinkage concrete by the stereo-microscope. Subsequently, a comparison is performed on the DRI of the concrete samples

held at distinct relative humidity levels, considering respectively the low and high concrete maturity conditions. Finally, it discusses the correlation between the DRI and Drying shrinkage and the drying shrinkage model is established to show the development of cracks at the different levels of drying shrinkage.

4.4 Experimental Procedure

4.4.1 Sample Preparation

A total of seventy-two, 100 mm by 200 mm, cylindrical concrete specimens were fabricated in the laboratory (i.e., 40 for each of the 38 ℃ group and 32 for the 60 ℃ group). The concrete mixture as shown in was Table 4.1 prepared with conventional GU cement, nonreactive coarse and fine aggregates. Hence, only drying shrinkage was considered. Also, each moisture/temperature condition consists of 8 specimens with 2 buckets containing 4 specimens each as shown in Figure 4.1.

Table 4.1Mix Proportion of the Concrete Specimens

Ingredients	Weight (kg)	Specific Gravity
Cement	420.00	3.15
Coarse Aggregate	1002.45	2.79
Fine Aggregate	852.05	2.74
Water	186.15	1

Figure 4.1 A Family Under the Same Exposed Condition

4.4.2 Fabrication, Cutting and Polishing

Cylindrical concrete specimens (100 mm diameter and 200 mm height) were cast. After casting, the specimens were demolded and moist cured at room temperature for 48 hours; holes were drilled on both sides and studs were installed using a fast-setting cement slurry during the first 24 hours. The initial length readings were conducted after 48 hours, and specimens were ready for storage. Next, each family was stored at numerous temperatures and relative humidity conditions as shown in Table 4.2; thereby inducing the drying shrinkage which was then monitored over time.

Table 4.2 The Different Exposure Conditions

Temp (°C)/RH (%)	**100**	**90**	**82**	**75**	**62**
38	100%-38°C	90%-38°C	82%-38°C	75%-38°C	62%-38°C
60		90%-60°C	82%-60°C	75%-60°C	62%-60°C

After 6 months, concrete specimens were longitudinally cut in half. One half underwent polishing with a polish pad which the size number is from 50 (coarse) to 3000 (very fine)

[5]. These polished specimens were inspected at 16x magnification for scratches. Any scratched surfaces required re-polishing, and all specimens were cleaned after each pad's use to remove abrasive residues.

4.4.3 Control and Measurement of Relative Humidity

One of the widespread methods for controlling relative humidity and temperature for experiments requiring a controlled environment is the use of environmental chambers which are expensive and could also delay other experimental works. Its use becomes more complicated given the number of samples and different moisture conditions needed for this research. As a result, the traditional method of controlling RH with the aid of saturated salt solutions as described in ASTM E104 [6] was adopted. Table 4.3 shows all the salt solutions used to achieve all the moisture and temperature combinations.

Table 4.3 Salt solution and RH conditions

Temp/RH	62%	75%	82%	90%	100%
38°C	sodium nitrite	sodium chloride	potassium chloride	potassium nitrate	distilled water
60°C	sodium nitrite	sodium chloride	potassium nitrate	potassium sulfate	

Water/saturated salt solution is placed in the bottom of each container for all conditions as highlighted in Table 4.3 and concrete specimens were stored on a perforated rack above the water/saturated salt solution. The relative humidity in each container was monitored over time with the aid of ibutton sensors, which was selected for this study due to their ability to function and save data independently without needing a data logger.

4.4.4 DRI Analysis

The damage rating index was originally designed to evaluate the damage in the concrete caused by the coarse aggregates [5]. With the development of DRI on the internal swelling mechanism, such as ASR, DEF, and FT, the use of DRI become the comprehensive microscopic assessment to evaluate the extent and cause of damage from either aggregate and cement paste mechanisms [1–2, 4, 5–7]. In this study, the use of DRI aims to observe and quantify the crack feature due to drying shrinkage. Therefore, the DRI is conducted using a stereomicroscope with a magnification of 16x. Figure 4.2 illustrates the quantification of these damage features achieved by observing a polished concrete sample using a mesh measuring 1 cm^2 , which is composed of individual units measuring 10 x 10 mm and covers the whole polished surface. As shown in Table 4.4, weighting factors are assigned to each damage feature based on their relative importance [5].

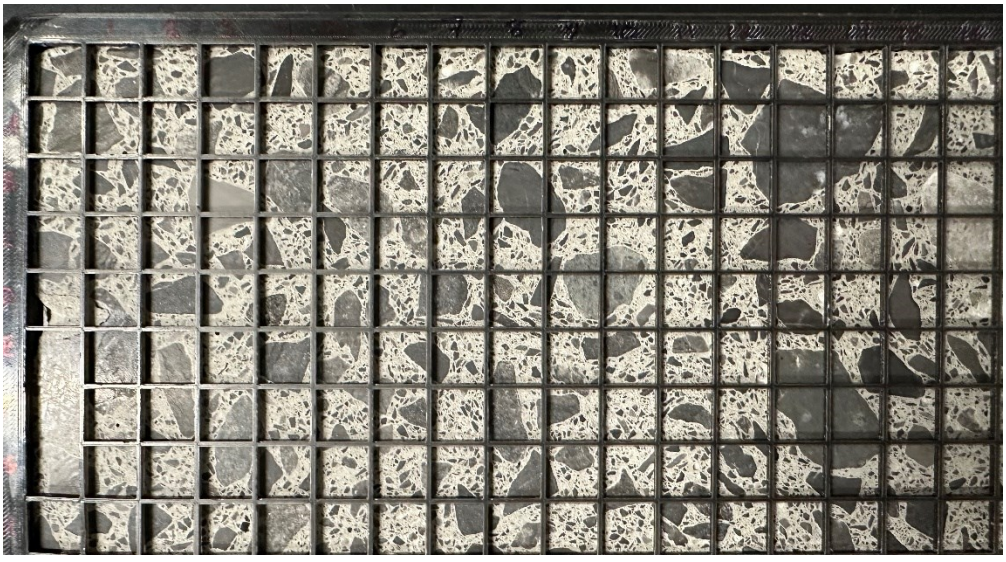

Figure 4.2 The Mesh on DRI Specimen

Table 4.4 Weighing Factors of DRI [9]

Cracks Feature	Abbreviation	Weighing factor
Cracks in coarse aggregate	**CCA**	0.25
Open cracks in coarse aggregate	**OCA**	2
Open cracks with reaction product in coarse aggregate	**OCAG**	2
Coarse aggregate debonded	**CAD**	3
Disaggregate/corroded aggregate particle	**DAP**	3
Cracks in cement paste	**CCP**	2
Cracks with reaction product in cement paste	**CCPG**	2

The main types of cracks observed in these specimens pertain to CCA, OCA, and CCP, as the aggregate components exhibit the degree of non-reactivity mentioned in CSA A23.2-27A, thereby avoiding the alkali-silica reaction (ASR) in this research. The damage features highlighted in Table 4.4 were used as a guide to counting the cracks in the concrete specimen of drying shrinkage; meanwhile, the pores and interfacial transition zone (ITZ) are crucially introduced for the development of drying shrinkage [8–13].

In this study, it is noted that the induced CCP resulting from drying shrinkage is observed to be thin, even when utilizing a stereo microscope with a magnification of 16x. Consequently, modifications are made to the DRI procedure. 1) Checking the CCP's state while using a high magnification level of 20x, considering the different types of CCP and solving if the uncertainty of the CCP surrounding or cutting through the aggregates occurs, 2) confirming the condition of the CCP by reverting to a magnification level of 16x, as the concept of DRI based on crack observations at this specific magnification.

4.4 Results

4.4.1 Drying Shrinkage Results

The change in length attained by concrete specimens subjected to two temperature groups (i.e., 38℃ and 60℃) and five distinct relative humidity (i.e., 100%, 90%, 82%, 75%, and 62%) are as shown in Figure 4.3 (a) and (b).

In the case of the 38℃ group, the specimens at relative humidity 90%, 82%, 75%, and 62% attained a maximum drying shrinkage level of -0.0195%, -0.0428%, -0.0488%, -0.00663% respectively at the concrete maturity of 6480 degree-days. Also, the specimen at 100% RH attained an expansion of 0.0191%. In the other case of the 60℃ group, all specimens reach a longer concrete maturity due to the temperature. The specimens with different relative humidity (i.e., 82%, 75%, 62%) reach the maximum drying shrinkage level (i.e., -0.0287%, -0.0416%, -0.0676%) at the concrete maturity of 10800 degree-days. Also, the specimen at 90% RH experiences an expansion of 0.0108%.

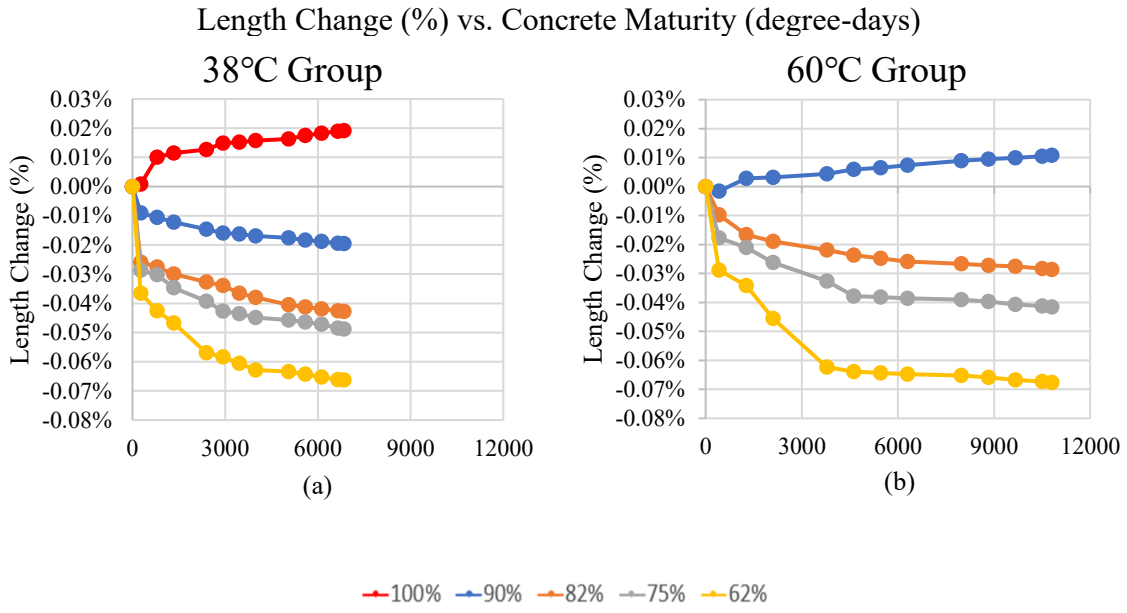

Figure 4.3 Length Change According to the Concrete Maturity (Degree-days); Concrete Maturity is the X-axis for these two figures above.

In Addition, these two exposure conditions of RH 100% at 38℃ and RH 90% at 60℃ manifest the expansion behaviour during the drying shrinkage measure. Considering the specimens stored at 100% RH and 38℃, an expansion was recorded despite the non-reactivity of the aggregates. The expansion is within the stated limits of the permitted expansion, as specified by CSA A23.2-27A. These limits are set at 0.040% after one year. Also, the length of the specimen at RH 90% and 60℃ reduces at the concrete maturity of 420 degree-days and then expands thereafter. It explains that the concrete, in this case, undergoes drying shrinkage at an early age because of water loss but then expands. However, its ultimate expansion meets the requirements set in the CSA A23.2-27A.

4.4.3 Amount of CCP

The presence of CCP is observed near the ITZ and pores in the microstructure of concrete while using a stereo microscope for DRI on the concrete specimens of drying shrinkage. This study does not only investigate the drying shrinkage behaviour of the cement paste. but is also able to comprehend the influence of these pores and ITZ on drying shrinkage. Therefore, the cracks in the cement paste (CCP) are divided into three types shown in Figure 4.4.

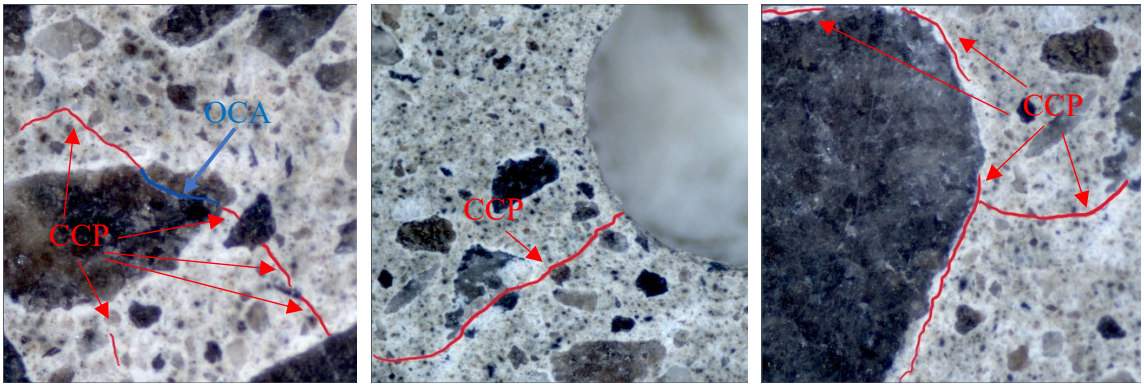

Typical CCP CCP at the Pore CCP at the ITZ

Figure 4.4 Three Types of CCP

Figure 4.5 (a) and (b) illustrate the amount of the three types of CCPs generated at distinct relative humidity at the low (38℃) and high (60 ℃) concrete maturity.

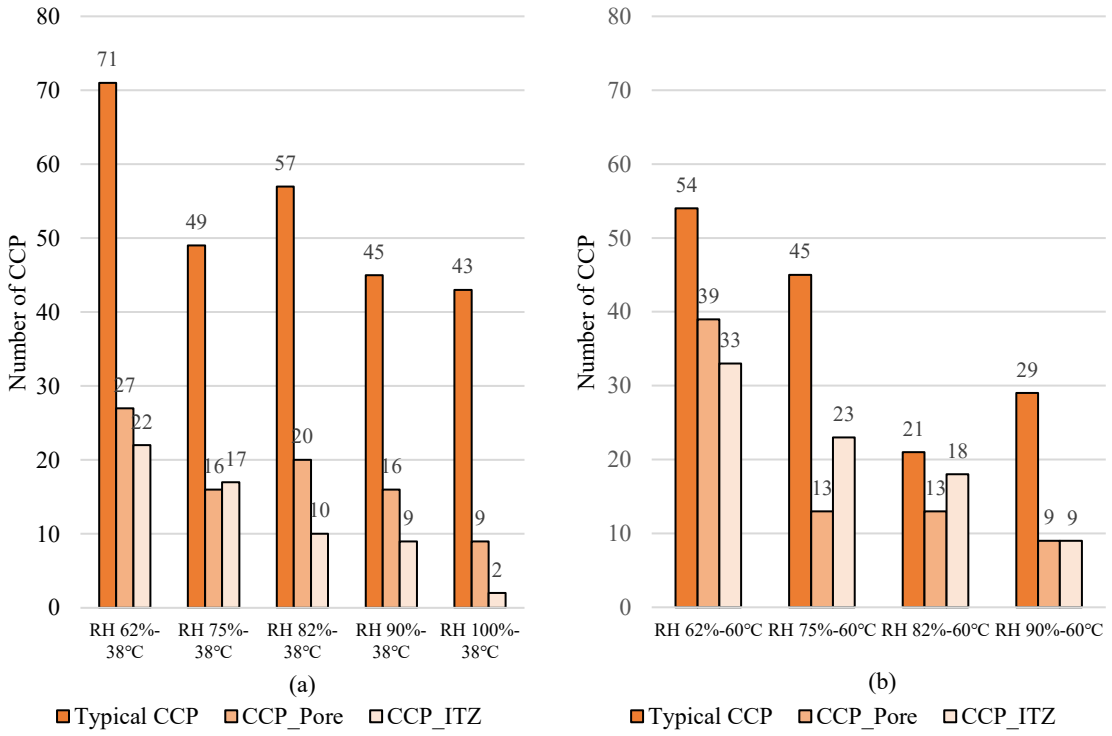

Figure 4.5 The Numbers of Three Types of CCP of (a) the 38℃ group, (b) the 60℃ group

At low concrete maturity, the specimen stored at 62%RH-38℃ has the most of all three types of CCPs (Typical CCP: 71, CCP_Pore;27, CCP_ITZ: 22). The difference in typical CCPs among RH 75%-38℃, RH 90%-38℃, and RH 100%-38℃ is not clear. The rise in the number of CCPs connected to pores exhibits a minimal effect of drying shrinkage on the pores in the concrete at lower relative humidity conditions, in contrast to the variation observed in the number of typical CCPs. When the concrete specimen is subjected to 100% RH, only a few CCPs are found in the interfacial transition zone (ITZ). However, when the relative humidity decreases, the amount of these specific CCPs approaches the CCPs present in the pores.

At the high level of concrete maturity, as the relative humidity decreases, there is an observed increase in the number of typical CCPs from 29 to 54, also, the biggest increase occurred at 75% relative humidity. Similarly, the amount of CCPs in the interfacial transition zone (ITZ) grows from 9 to 33, while the amount of CCPs connecting to the pores increases from 9 to 39. Nevertheless, until the relative humidity dropped to 62%, fewer CCPs were merging with the pores than there were in the ITZ.

4.4.2 DRI Result

Figure 4.6 and Figure 4.7 illustrates the DRI number for the concrete specimen under different exposure conditions.

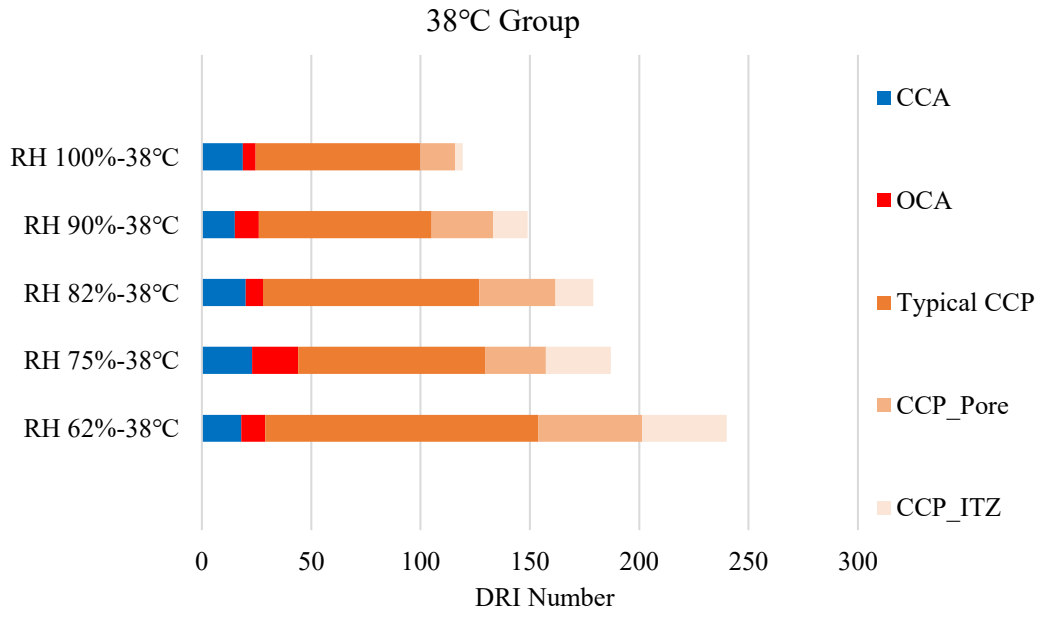

Figure 4.6 DRI of 38℃ Group

In the case of the 38℃ group, Figure 4.6 illustrates the DRI number increases with a decrease in the relative humidity. The specimen stored at 100% RH-38℃ attained the lowest DRI number (119) and the specimen stored at 62% RH-38℃ attained the highest

DRI number (239). These specimens with a relative humidity of 82% and 75% attained the closed DRI numbers of 179 and 187, respectively. Furthermore, the DRI values for specimens with relative humidity of 100% (119) and 90% (148) exhibit a range below 150 but above 100. Similarly, the DRI values for specimens with a relative humidity of 82% (179) and 75% (187) are below 200 but above 150. Lastly, the DRI values for specimens with a relative humidity of 62% (239) are below 250 but above 200.

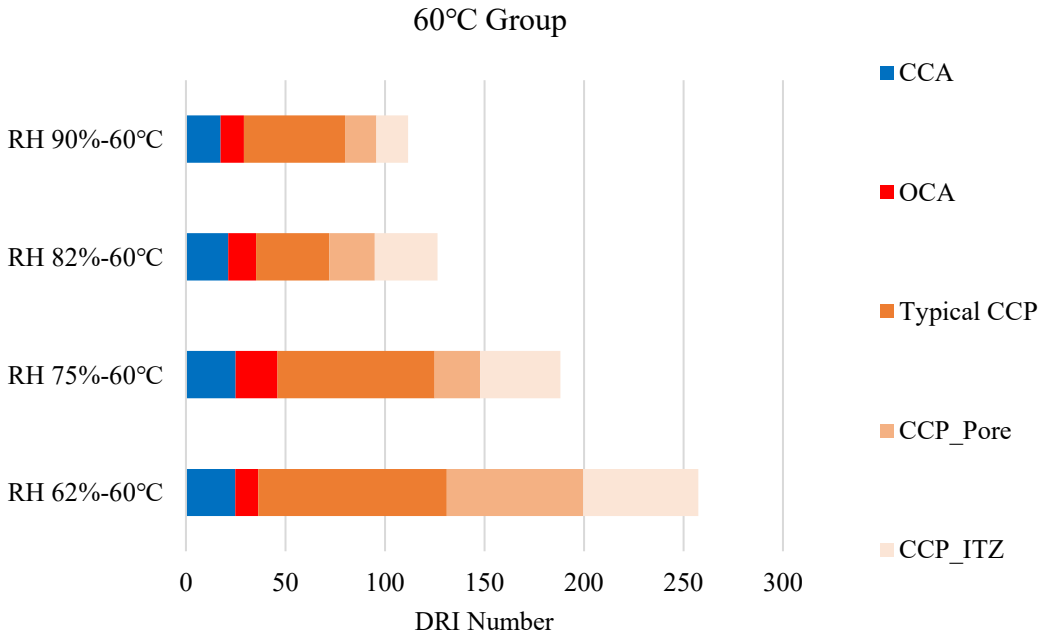

Figure 4.7 DRI of 60℃ Group

Figure 4.7 illustrates the DRI number of the specimen with four distinct relative humidity (i.e., 90%, 82%,75%, and 62%) stored at 60℃. Similarly, the DRI number increases with the decrease of relative humidity. The specimen stored at 90%RH-38℃ attained the lowest DRI number (112) and the specimen of RH 62%-38℃ attained the highest DRI number (257). In 60℃, the DRI values for specimens with a relative humidity of 90% (112) and 82% (126) exhibit a range below 150 but above 100; the DRI values for specimens with a

relative humidity of 75% (188) are below 200 but above 150. Lastly, the DRI values for specimens with a relative humidity of 62% (257) are below 250 but above 200.

4.5 Discussion

4.5.1 Correlation between Damage Rating Index and Drying Shrinkage

Figure 4.8 illustrates the DRI numbers of the concrete specimens stored at distinct relative humidity at 38ºC. The DRI number exhibits a trend of increase when the relative humidity decreases at similar concrete maturity as shown in Figure 4.3 (a). In the meantime, it has been observed that the DRI value is closely associated with the drying shrinkage of the specimens. For instance, the drying shrinkage for RH 82%-38℃ and RH 75%-38℃ is -0.0428% and -0.0488%, respectively, presenting DRI number of 179 and 187. Among all three types of CCPs, the amount of the typical CCP, which does not connect to pores nor ITZ, is most significant in the DRI number for all exposure conditions. The CCP influencing the pores is the medium in the total CCP and it slightly increases with the development of drying shrinkage. Then, the CCP at ITZ is the smallest part of the total CCP; fewer number was counted at 100% RH; however, it exhibits a significant increase when the specimen is subjected to decreased relative humidity. Also, CCA (closed cracks in the aggregate) and OCA (opened cracks in the aggregate) obtained a small portion of the total DRI number. In this research, the aggregate is categorized as non-reactivity to the ASR but still performs a very low expansion (< 0.040% in one year according to CSA A23.2-27A), therefore, ASR affects less on the aggregates and forms few CCA and OCA.

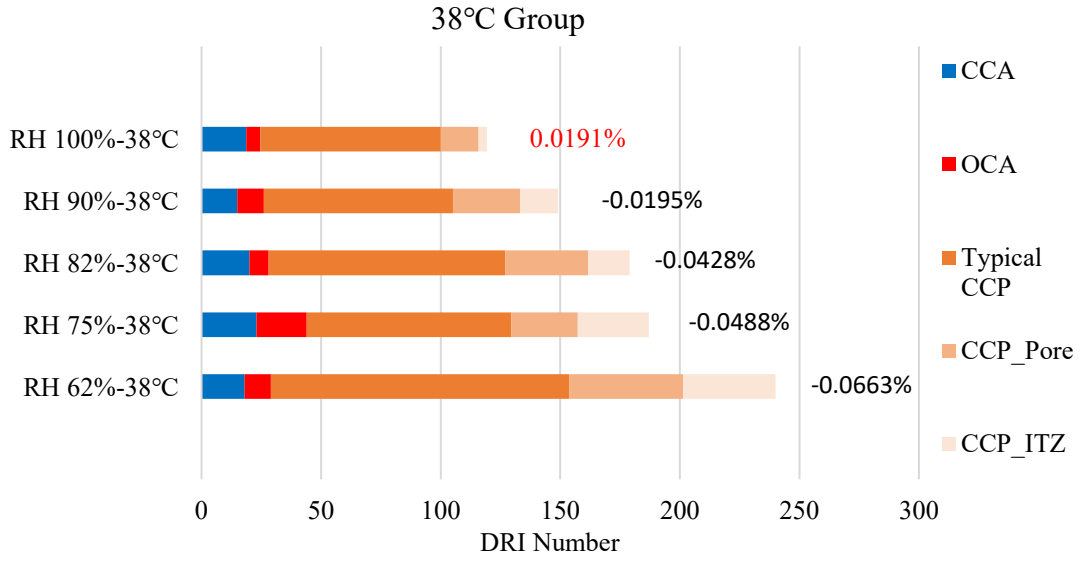

Figure 4.8 DRI Number for Drying Shrinkage Specimens of the 38°C Group with Length Change Results

Figure 4.9 illustrates the DRI number of the concrete specimens undergoing the different relative humidity stored at 60ºC. At a higher level of concrete maturity, illustrated in Figure 4.12 (b), there is a pronounced increase in the DRI number. Furthermore, it is noted that the difference between high and low relative humidity is more prominent; for instance, there is a significant rise in the DRI value when the relative humidity (RH) decreases from 82% (DRI:126) to 75% (DRI:188) at a temperature of 60°C. Furthermore, the increasing proportion of CCPs connecting to the pores and CCPs at the ITZ becomes more noticeable when the relative humidity decreases from 82% to 62%. Furthermore, the specimen stored at 62% RH-60ºC exhibits a considerable increase in CCP that is connected to the pores and ITZ; the specimen stored at 75%RH-60°C also demonstrates significant growth on a typical

CCP. In addition, although the amount of CCA and OCA obtained a minor part of the total DRI, it slightly increases at the high concrete maturity.

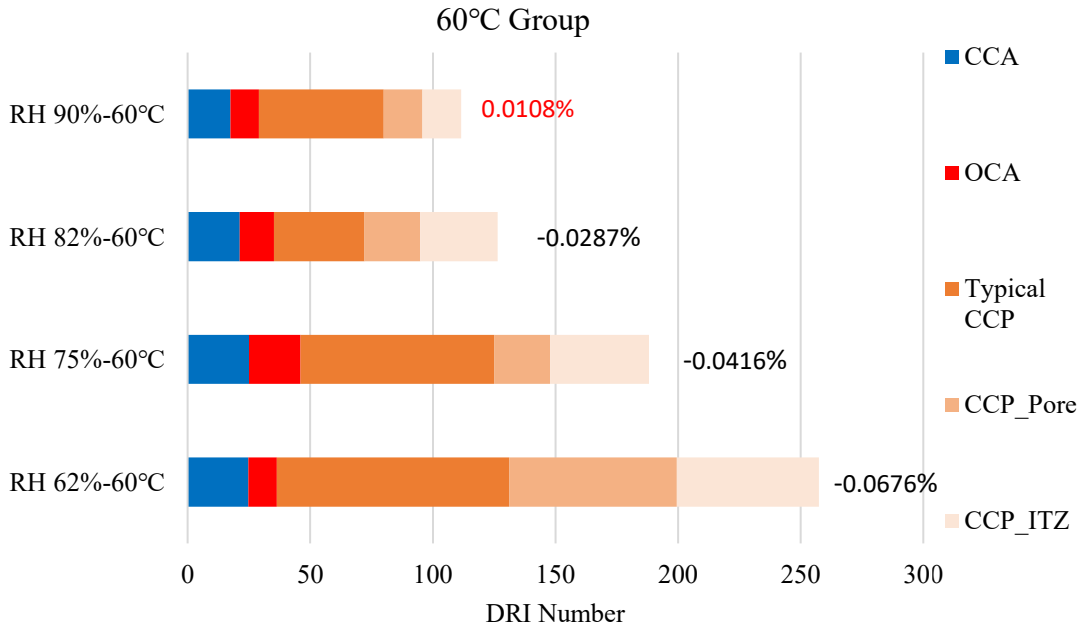

Figure 4.9 DRI Number for Drying Shrinkage Specimens of the 60°C Group with Length Change Results

Figure 4.8 and Figure 4.9 illustrate the tendency of increasing the DRI number of CCP and the total DRI number is proved by the increase in drying shrinkage by rearranging the magnitude of drying shrinkage for all exposure conditions in an ascending order.

4.5.2 Proportions and Amounts of Three Types of CCPs

Figure 4.10 (a) and (b) show the proportion of three types of CCP in the groups of two distinct temperature groups. In the 38°C group, which presents the low concrete maturity in Figure 4.12 (a), it was found that the typical CCPs dominate the majority (about 60%) of total CCP formation. Moreover, with the decrease of the relative humidity from 100% to 62%, the proportion of the CCP decreases (from 79.63% to 59.17%); in contrast, the growth in the proportion of CCPs which is associated with the pores (from 16.67% to

22.50%) and ITZ (from 3.70% to 18.33%) is measured. In the 60℃ group, which is the high concrete maturity, the proportions of these three CCPs tend to be balanced. Despite the specimen stored at 90%RH-60℃ having performed the expansion behaviour, the total proportion of CCP associated with the pores and ITZ increased to at least 40% in the other three specimens in the 60℃. Significantly, the total proportion of CCP associated with the pores and ITZ reaches more than 50%, which means the influences of pores and ITZ on CCPs also become more significant.

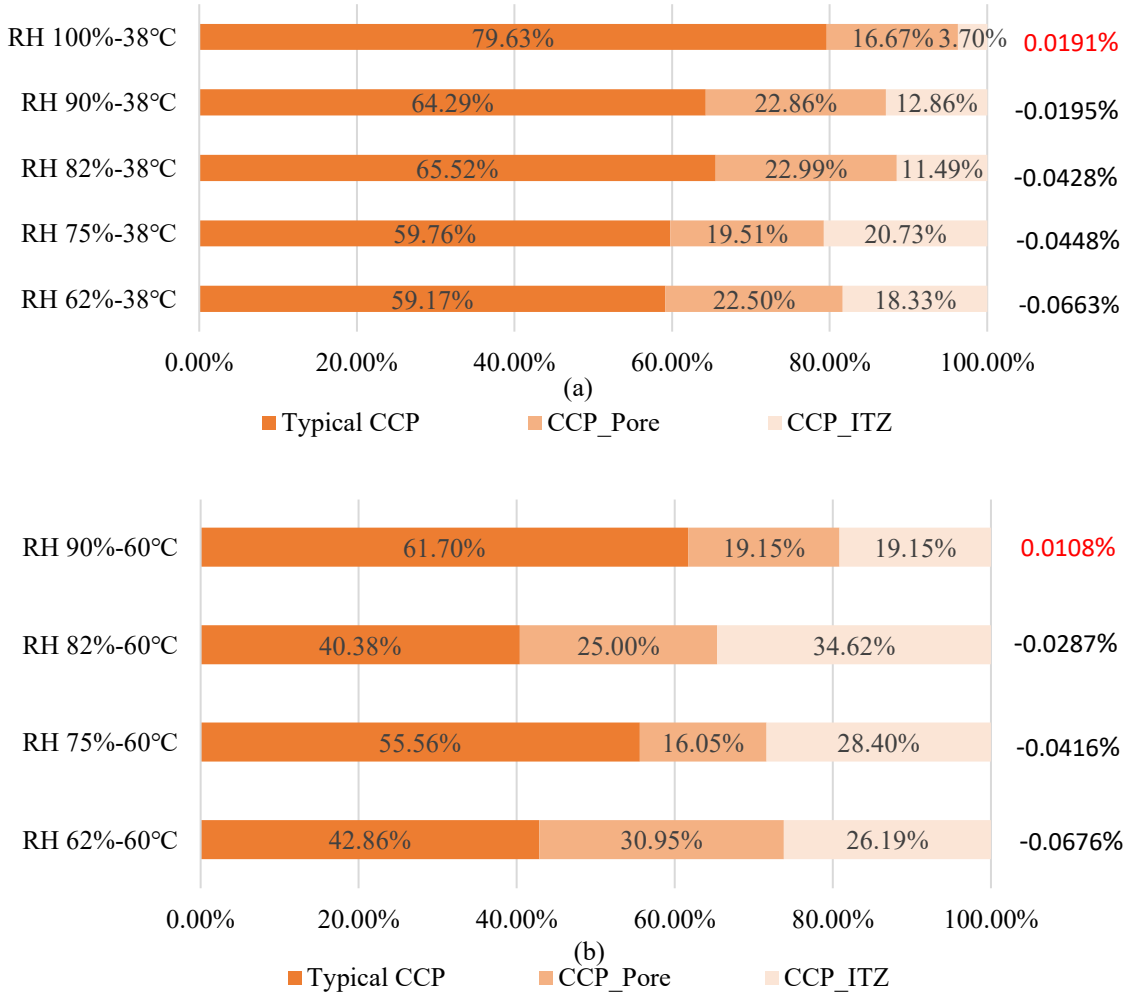

Figure 4.10 The Percentage of Different Types of CCP Induced by Drying Shrinkage with the Length Change Results of (a) the 38℃ Group, (b) the 60℃ Group.

4.5.3 The Extent of Concentration of CCP on DRI

Table 4.5 (a) and (b) illustrate the influence of CCP, which is presented by the DRI number, on the polished surface of the specimens for both low (38℃ group) and high (60℃ group) concrete maturity. The utilization of the red-yellow-green colour scale is a prevalent approach that offers a visually comprehensible means of interpreting data. This method involves the application of a gradient of colours, ranging from red to yellow to green, to a set of cells, hence facilitating the assessment of their respective values. The colour red is commonly associated with the higher DRI values attributed to CCPs. The highest level of damage from CCPs within a given range of cells will be visually represented by the colour red, which signifies areas that require attention on many CCPs. The colour yellow is indicative of the average values within the data range of the DRI. This colour performs as an intermediary colour positioned between red and green, symbolizing the amount of CCP in each cell that is neither notably high nor low. The colour green is utilized to represent the lower values within the range of CCP on DRI. It often indicates that the 1 cm^2 surface cell is observed a lower amount of CCPs. The transition from red to green is gradual, passing through various shades of orange and yellow.

At low concrete maturity (the 38 ℃ group), as the relative humidity decreases, the presence of CCPs propagates and fills more of several cells on the concrete polished surface as shown in Table 4.6(a). Simultaneously, the greater amount of red and orange cells reflects the increase of CCPs, which indicates an increase in the damage caused by CCPs occurs at the surface because more and more water loss due to the low relative humidity induces more tensile stress in the hydrated cement paste so that the development of CCP get more pronounced under the stereomicroscope. When the relative humidity reaches 100%, it

manifests a few isolated collections of the CCPs within cells on the polished surface in Table 4.6 (a). As the relative humidity decreases to 75%, an increasing number of red and orange cells becomes considerable. Moreover, it shows that the area of CCP on the entire polished surface area increases to 38% at a relative humidity (RH) of 62%, whereas it is only 12% at an RH of 100%.

At the high concrete maturity (the 60℃ group), Table 4.6 (b) also presents the trend of expanding the distribution area of the CCP, as well as the corresponding rise in the number of cells illustrated by those experiencing severe CCP damage. For example, the distribution area of the CCP at a relative humidity of 62% constitutes 34% of the total polished surface area, in contrast to other specimens where the distribution areas at RH 90%, RH 82%, and RH 75% represent 15%, 18%, and 23% respectively.

Table 4.5 The DRI Number of CCP for Distinct Exposure Conditions in (a) 38℃ and (b) 60℃

RH100%-38℃	1	2	3	4	5	6	7	8	9	10	11	12	13	14	15	16	17	18	19
A	0	0	12	0	0	0	0	9	0	0	0	0	0	0	0	0	6	3	0
B	0	6	9	0	0	0	0	0	0	0	0	0	0	0	0	0	27	0	0
C	0	0	0	0	0	0	3	0	0	0	0	0	3	3	3	12	0	0	0
D	0	0	0	0	0	0	0	0	0	0	0	0	0	0	0	9	0	0	0
E	0	0	3	0	6	0	0	0	0	0	0	0	0	0	0	0	0	0	0
F	0	0	0	0	0	9	6	0	0	0	0	0	0	0	0	0	0	0	0
G	0	0	3	0	0	15	0	0	0	0	0	3	0	0	0	0	0	0	0
H	0	0	0	0	0	12	0	0	0	0	0	0	0	0	0	0	0	0	0
I	0	0	0	0	0	0	0	0	0	0	0	0	0	0	0	0	0	0	0
RH90%-38℃	1	2	3	4	5	6	7	8	9	10	11	12	13	14	15	16	17	18	19
A	0	0	0	0	0	0	0	3	0	0	0	0	0	0	0	0	6	3	3
B	0	0	0	0	0	0	3	6	0	3	6	0	3	0	0	15	0	0	0
C	0	0	6	0	3	0	0	0	0	0	3	0	9	0	0	0	3	0	0
D	3	0	0	0	3	12	9	0	3	0	3	0	0	9	0	0	0	0	0
E	0	3	0	0	6	0	0	0	0	3	0	9	0	0	0	0	0	3	0
F	0	0	0	0	3	3	3	6	0	12	6	0	0	0	0	0	0	3	0
G	0	0	0	3	0	0	0	3	0	6	3	0	0	0	0	0	0	0	0
H	0	0	0	0	0	0	0	0	3	0	3	0	0	0	0	0	0	3	0
I	0	0	0	0	0	0	0	6	0	0	0	0	0	0	0	0	3	0	0
RH82%-38℃	1	2	3	4	5	6	7	8	9	10	11	12	13	14	15	16	17	18	19
A	0	3	3	0	0	0	0	0	0	0	9	3	3	6	6	0	0	0	15
B	0	0	3	3	0	3	3	0	12	3	0	0	0	21	0	0	0	0	0
C	0	0	0	0	0	0	0	0	9	0	0	9	6	6	6	0	3	0	12
D	0	0	0	0	0	0	0	0	0	0	6	0	0	0	0	3	3	0	0
E	0	0	0	0	0	0	0	0	3	3	0	9	0	0	0	0	6	0	0
F	0	0	0	9	0	0	0	0	3	0	6	0	0	6	0	0	6	0	0
G	0	0	0	0	0	0	3	0	0	3	0	0	3	0	0	0	6	0	3
H	0	0	0	0	0	0	0	0	3	3	0	0	0	0	3	0	6	3	12
I	0	0	0	0	0	0	0	3	0	0	0	0	0	0	0	0	0	0	0
RH75%-38℃	1	2	3	4	5	6	7	8	9	10	11	12	13	14	15	16	17	18	19
A	0	0	0	3	3	3	0	3	0	0	3	0	0	0	6	0	0	0	0
B	0	6	0	0	0	0	6	0	0	3	0	0	0	0	3	0	3	0	0
C	0	0	0	0	0	9	6	0	0	0	9	0	0	0	3	0	0	0	3
D	0	0	0	0	0	3	6	0	0	0	0	0	3	0	6	0	0	0	0
E	0	0	0	0	0	0	3	0	9	0	0	6	0	12	0	0	0	0	0
F	0	0	0	0	0	0	0	0	12	6	0	0	3	0	0	3	0	9	0
G	0	0	0	0	3	0	0	0	15	0	0	0	0	0	0	0	0	0	9
H	0	0	0	0	0	0	0	12	0	0	0	0	0	0	0	0	0	3	0
I	0	0	0	3	0	6	0	0	0	0	0	6	3	9	0	12	3	6	3
RH62%-38℃	1	2	3	4	5	6	7	8	9	10	11	12	13	14	15	16	17	18	19
A	0	6	0	12	9	0	0	0	3	6	3	6	0	15	0	6	0	9	0
B	0	3	0	0	18	3	9	3	0	3	6	6	3	3	9	0	3	0	0
C	0	0	0	0	3	0	0	0	3	3	0	0	3	3	3	0	9	0	0
D	0	0	6	6	0	3	0	0	0	6	0	0	6	3	0	0	6	0	0
E	0	0	0	3	0	0	6	0	0	0	0	0	3	0	9	9	6	6	0
F	0	0	6	0	0	6	0	0	0	0	0	3	0	3	0	0	0	0	3
G	0	0	6	6	0	6	3	0	0	0	3	0	9	0	12	0	0	0	0
H	0	0	9	0	0	0	0	0	3	3	3	0	0	0	0	0	0	0	3
I	0	0	3	0	9	6	0	3	0	3	0	0	0	0	0	0	0	0	0

(a)

RH90%-60℃	1	2	3	4	5	6	7	8	9	10	11	12	13	14	15	16	17	18	19
A	0	0	0	0	0	0	0	6	0	0	0	9	6	0	3	3	0	0	0
B	0	0	6	0	0	0	0	0	0	9	0	0	0	0	0	3	3	0	0
C	0	0	0	0	0	0	0	0	0	3	6	0	0	0	0	0	0	0	0
D	0	0	0	0	6	0	0	6	0	3	0	0	0	0	0	0	0	0	0
E	0	0	3	3	0	0	0	0	0	0	0	0	0	0	0	0	0	0	0
F	0	0	3	3	0	6	0	0	0	0	0	0	0	12	0	0	0	0	0
G	0	0	0	0	3	0	0	0	0	3	0	0	0	0	0	3	0	0	0
H	0	6	0	0	0	0	3	0	0	0	0	0	3	0	0	12	0	0	0
I	0	0	0	0	3	0	0	0	0	0	0	3	0	0	0	0	0	0	0
RH82%-60℃	1	2	3	4	5	6	7	8	9	10	11	12	13	14	15	16	17	18	19
A	0	0	0	0	0	0	3	0	0	0	0	0	0	0	0	0	3	0	0
B	0	0	0	3	3	6	6	0	0	12	0	0	0	0	6	3	0	0	0
C	0	0	0	0	0	0	3	0	3	0	0	6	0	0	6	3	3	0	0
D	0	0	0	6	0	0	0	6	6	0	0	0	0	0	3	0	0	0	0
E	0	0	0	0	9	3	0	0	0	0	3	0	0	0	0	6	0	3	0
F	0	0	0	0	0	0	18	0	0	0	0	0	0	0	0	0	0	0	0
G	0	0	0	0	0	0	0	0	0	0	0	0	0	3	0	0	0	0	0
H	0	6	0	0	0	0	0	0	0	0	0	0	0	3	0	0	0	0	0
I	0	0	0	0	0	0	6	0	0	0	6	0	0	0	0	0	0	0	0
RH75%-60℃	**1**	**2**	**3**	**4**	**5**	**6**	**7**	**8**	**9**	**10**	**11**	**12**	**13**	**14**	**15**	**16**	**17**	**18**	**19**
A	**0**	**0**	**0**	**0**	**0**	**0**	**0**	**15**	**0**	**0**	**0**	**0**	**3**	**0**	**0**	**9**	**0**	**3**	**0**
B	**0**	**0**	**6**	**0**	**0**	**0**	**0**	**0**	**6**	**0**	**0**	**6**	**0**	**9**	**6**	**0**	**0**	**0**	**0**
C	**0**	**0**	**9**	**0**	**0**	**0**	**0**	**0**	**3**	**9**	**3**	**9**	**0**	**0**	**12**	**0**	**0**	**0**	**3**
D	**0**	**0**	**0**	**0**	**0**	**0**	**0**	**3**	**0**	**15**	**0**	**0**	**3**	**0**	**0**	**0**	**0**	**0**	**0**
E	**0**	**0**	**0**	**9**	**0**	**6**	**0**	**0**	**0**	**0**	**0**	**0**	**0**	**0**	**6**	**6**	**0**	**0**	**3**
F	**0**	**0**	**3**	**9**	**0**	**0**	**6**	**0**	**0**	**0**	**0**	**9**	**0**	**0**	**3**	**12**	**0**	**3**	**0**
G	**0**	**0**	**0**	**3**	**0**	**6**	**0**	**0**	**0**	**0**	**0**	**3**	**0**	**0**	**0**	**0**	**0**	**3**	**0**
H	**0**	**0**	**0**	**0**	**3**	**6**	**0**	**0**	**0**	**0**	**0**	**0**	**0**	**6**	**0**	**0**	**0**	**0**	**0**
I	**0**	**0**	**0**	**0**	**0**	**0**	**0**	**0**	**0**	**3**	**0**	**0**	**0**	**0**	**0**	**0**	**0**	**3**	**0**
RH62%-60℃	1	2	3	4	5	6	7	8	9	10	11	12	13	14	15	16	17	18	19
A	0	0	0	3	0	0	3	0	0	0	9	0	0	6	3	0	6	0	0
B	0	0	0	0	0	6	0	3	0	6	0	0	0	3	6	12	3	9	15
C	0	0	9	0	6	0	3	3	0	3	0	0	0	9	0	3	0	12	0
D	0	0	0	0	6	0	0	0	0	0	0	0	0	0	0	6	0	12	0
E	0	0	6	3	0	6	0	9	3	0	0	0	0	0	0	3	0	0	0
F	0	0	0	0	0	3	0	9	6	0	3	0	0	3	12	0	0	3	0
G	0	0	0	15	0	6	3	9	12	9	0	12	6	0	0	0	0	9	0
H	0	0	0	3	0	9	3	0	0	0	0	0	0	0	0	0	0	0	21
I	0	0	0	0	3	0	0	3	0	0	0	6	0	3	0	6	0	0	6

(b)

Table 4.6 illustrates the occurrence of different amounts of CCP in the cells at the low concrete maturity (i.e., the 38℃ Group). The correlation between the damage caused by CCP and relative humidity is evident because a greater number of damages from CCP is associated with a drop in relative humidity.

Table 4.6 The CCP Amount Observed Within One Cell Under the Different Exposure Conditions in the 38℃ Group

RH (%) / The CCP amount observed within the cell	**1**	**2**	**3**	**4**	**5**	**6**	**7**	**8**	**9**	Total CCP
100	8	4	4	3	1				1	54
90	27	9	4	2	1					70
82	24	12	5	3	1		1			87
75	21	11	6	4	1					82
62	31	20	10	2	1	1				120

In comparison to the specimen with 100% relative humidity (i.e., the expansion of 0.0191%), the specimens observed the drying shrinkage (e.g., 90% RH manifests the drying shrinkage of -0.0195%) exhibits more amount of the cells containing one CCP. It is important to state drying shrinkage generates more CCPs at the identical magnitude of the length change while decreasing relative humidity from 100% RH. Compared to the specimens with relative humidity of 82% and 75%, the data of various CCP amounts within each cell are closed because the drying shrinkage (-0.0428% and -0.0488%) of these two exposure conditions are closed as well. Significantly, the concrete specimen subjected to a relative humidity of 62% exhibits a considerable observation on most cells containing one, two, or three CCPs. It means that the extent of drying shrinkage on concrete increases so

that more and more cells, which do not contain CCP or observe no more than three CCP at the higher relative humidity, are observed in the formation and increasing of CCP instead of those cells that have already shown the loss of CCPs, compared with the other relative humidity (i.e., 90%, 82%, and 75% RH).

Table 4.7 The CCP Amount Observed Within One Cell Under the Different Exposure Conditions in the 60℃ Group

RH (%) / The CCP amount observed within the cell	**1**	**2**	**3**	**4**	**5**	**6**	**7**	**8**	**9**	Total CCP
90	17	8	2	2						47
82	15	12	1	1		1				52
75	15	11	8	2	2					81
62	23	16	10	6	2		1			126

Table 4.7 illustrates the various CCP accounts observed within cells in high concrete maturity (i.e., the 60℃ group). Compared to the higher relative humidity condition (i.e., 90%), the specimen stored at the relative humidity of 82% and 75% attained the closed data on the amount of cells observed the one or two CCPs because CCPs generated when it also underwent drying shrinkage at the initial period shown in Table 4.5 (b). However, the difference in relative humidity between 82% and 75%, which demonstrates distinct levels of drying shrinkage (-0.0287% and -0.0416% respectively), indicates the number of cells observed in at least three CCPs at the high concrete maturity. In the condition of 82% relative humidity, six CCPs occurred within one cell. Nevertheless, an increase in the amount of CCPs (varying from three to five) within the cell was found under the condition of 75% relative humidity. In this case, the effect of temperature accelerates the rate of water evaporation, leading to a pronounced magnitude of drying shrinkage. At higher concrete

maturity, the formation of CCPs becomes challenging in cells that do not contain any CCPs at lower relative humidity; instead, drying shrinkage continues to develop CCPs within these cells that have already deteriorated by many CCPs. Significantly, when the relative humidity is at 62%, the specimen does not only exhibit a cell observed indicating the presence of 7 CCPs but also presents the most cells that manifest high damage from CCP in terms of many CCPs within the cell (i.e., the number of cells observed more than 2 CCPs).

4.5.4 Descriptive Drying Shrinkage Model

Based on the results in Figure 4.5 (a), drying shrinkage-induced cracks (CCPs) increases as the relative humidity increases. Furthermore, there exists a trend in the formation of the three types of CPs based on the exposed RH. Considering this finding, a descriptive model was proposed as shown in Figure 4.11 to illustrate the development of the three types of CCPs over drying shrinkage progress. To give a pictorial representation of such developments, the typical CCPs as represented as red, the CCP at the pores as green, while the CCPs at ITZ are represented as blue.

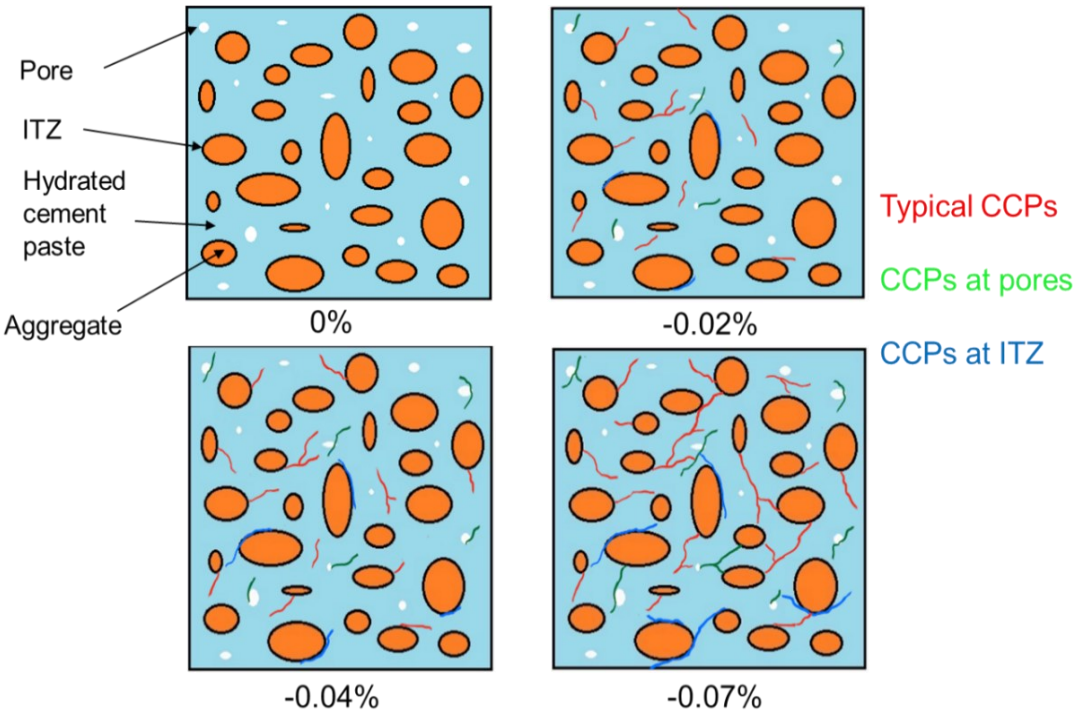

Figure 4.11 Descriptive Drying Shrinkage Damage Model vs. Levels of Drying Shrinkage between 0% and -0.07% in the 38°C Group

At a low drying shrinkage level (i.e., around -0.02%), most CCPs are from typical CCPs, also, the amount of CCP at the pores or ITZs attained a small proportion of the total CCPs. The length of these CCPs is short and the width is thin. Meanwhile, typical CCPs are randomly located in the concrete and are observed either at the cement paste or close to the aggregate. Moreover, few typical CCPs show crack branching as compared to cracks observed at high levels of drying shrinkage.

At the moderate level of drying shrinkage (i.e., round -0.04%), further propagation of these CCPs was observed. The length of these CCPs extends to approach the aggregate and the CCPs nearby. Significantly, the new typical CCPs with tiny sizes are observed at the original typical CCPs to form the crack branching. Furthermore, the increased amount of CCPs at pores and ITZs is low compared to that of typical CCPs. Moreover, the

development of these cracks mostly focuses on the propagation of existing CCPs rather than the generation of new CCPs. Hence, it can be observed that the ends of these CCPs located at the pores and ITZs grew in length.

At the high level of drying shrinkage (i.e., around 0.07%), the network of CCPs is observed in concrete. There exists a great increase in the number of typical CCPs, and the length and width of CCPs become longer and wider. Furthermore, the three types of CCPs extend towards the edges of these aggregates and interact with one another, resulting in the development of additional crack branching within the concrete. Additionally, the formation of CCPs within ITZs not only creates new cracks within the ITZs of these aggregates but also tends to grow in length along the ITZs and surround the aggregates.

4.6 Conclusion

The purpose of the study is to know whether the damage rating index can evaluate the damage extent and cracks features of the drying shrinkage mechanism in concrete. Meanwhile, DRI can provide more details on the propagation of cracks (CCP) in the cement paste while decreasing the relative humidity of concrete; also, the correlation between the CCP and the pores and ITZ in concrete is established. Some conclusions are presented below:

- DRI numbers become greater when the concrete is exposed to conditions with low relative humidity. Meanwhile, when the concrete specimens with the same concrete maturity obtained the closed drying shrinkage, their DRI number can be determined in a certain range.
- When the level of concrete maturity is low, the primary factor responsible for causing damage to the concrete is the typical CCP that does not connect to the pores

or ITZ. Nevertheless, at the high concrete maturity, the factors of drying shrinkage related to pores and ITZ become of greater importance in determining the total amount of CCPs.

- At the low concrete maturity, drying shrinkage generates more CCPs in concrete at the identical magnitude of the length change of the expansion as decreasing relative humidity from the saturated condition. Meanwhile, the similar magnitude of drying shrinkage causes a similar amount of CCPs. Significantly, the effect of drying shrinkage occurring at the low concrete maturity (i.e., 38°C) focused on the generation of more initial CCPs; also, the effect of drying shrinkage occurring at the high concrete maturity (i.e., 60°C) focuses on developing the existing CCPs.
- The development of CCP induced by drying shrinkage does not only illustrate the increases in area that observed CCP on the polished surface but also can present a high degree of CCP concentration when the specimens are exposed to low moisture conditions.

4.7 References

[1] L. F. M. Sanchez, T. Drimalas, B. Fournier, D. Mitchell, and J. Bastien, 'Comprehensive damage assessment in concrete affected by different internal swelling reaction (ISR) mechanisms', *Cement and Concrete Research*, vol. 107, pp. 284–303, May 2018, doi: 10.1016/j.cemconres.2018.02.017.

[2] L. F. M. Sanchez, T. Drimalas, and B. Fournier, 'Assessing condition of concrete affected by internal swelling reactions (ISR) through the Damage Rating Index (DRI)', *Cement*, vol. 1–2, p. 100001, Jun. 2020, doi: 10.1016/j.cement.2020.100001.

[3] H. N. Walker, ‘Petrographic Methods of Examining Hardened Concrete: A Petrographic Manual’, 1997, doi: 10.21949/1404099.

[4] P. K. Mehta and P. J. M. Monteiro, *Concrete: microstructure, properties, and materials*, 3rd ed. New York: McGraw-Hill, 2006.

[5] L. Sanchez, B. Fournier, M. Jolin, J. Bastien, D. Mitchell, and M. Noel, ‘The Use of the Damage Rating Index (DRI) for The Condition Assessment of Aging Distressed Concrete’, in *16th International Conference on Alkali-Aggregate Reaction*, Brazil, 2016.

[6] D22 Committee, ‘Practice for Maintaining Constant Relative Humidity by Means of Aqueous Solutions’, ASTM International. doi: 10.1520/E0104-20A.

[7] L. F. M. Sanchez, B. Fournier, M. Jolin, D. Mitchell, and J. Bastien, ‘Overall assessment of Alkali-Aggregate Reaction (AAR) in concretes presenting different strengths and incorporating a wide range of reactive aggregate types and natures’, *Cement and Concrete Research*, vol. 93, pp. 17–31, Mar. 2017, doi: 10.1016/j.cemconres.2016.12.001.

[8] A. Zahedi, C. Trottier, L. F. M. Sanchez, and M. Noël, ‘Microscopic assessment of ASR-affected concrete under confinement conditions’, *Cement and Concrete Research*, vol. 145, p. 106456, Jul. 2021, doi: 10.1016/j.cemconres.2021.106456.

[9] L. F. M. Sanchez, B. Fournier, M. Jolin, and J. Duchesne, ‘Reliable quantification of AAR damage through assessment of the Damage Rating Index (DRI)’, *Cement and Concrete Research*, vol. 67, pp. 74–92, Jan. 2015, doi: 10.1016/j.cemconres.2014.08.002.

[10] I. Maruyama, ‘Origin of Drying Shrinkage of Hardened Cement Paste: Hydration Pressure’, *ACT*, vol. 8, no. 2, pp. 187–200, Jun. 2010, doi: 10.3151/jact.8.187.

[11] B. Menu, M. Jolin, and B. Bissonnette, ‘Studies on the Influence of Drying Shrinkage Test Procedure, Specimen Geometry, and Boundary Conditions on Free Shrinkage’, *Advances in Materials Science and Engineering*, vol. 2017, pp. 1–9, 2017, doi: 10.1155/2017/9834159.

[12] J. P. Ollivier, J. C. Maso, and B. Bourdette, ‘Interfacial Transition Zone in Concrete’.

5. Chapter Five: Conclusion and Recommendations

This research aims to study the drying shrinkage mechanism on hardened state concrete and assess the efficiency of using DRI to evaluate the deterioration of drying shrinkage on concrete with distinct relative humidity. The standardized test on drying shrinkage is modified based on the original design for the ASR mechanism according to the distinct relative humidity. The physical properties of concrete undergoing drying shrinkage are observed and measured in terms of length change, mass loss, elastic modulus, and porosity. Meanwhile, many research studies have applied microscopic technology to investigate the drying shrinkage behaviour on the microstructure of concrete, such as SEM and DIC, but the damage features and extent of drying shrinkage are not fully presented. Therefore, this research provides some conclusions to explain the drying shrinkage behaviours on concrete and evaluate the development of CCP in the distinct relative humidity conditions (100%, 90%, 82%, 75%, and 62%) at two temperatures (i.e., 38℃ and 60℃).

- The drying shrinkage increases in the concrete when it is exposed to low relative humidity. Meanwhile, the concrete subjected to a lower temperature (i.e., 38℃) exhibits a greater magnitude of length change when exposed to high relative humidity, specifically those at 90%, 82%, and 75%, compared to the concrete subjected to a higher temperature (i.e., 60℃). However, at the same concrete maturity, the concrete specimens with identical relative humidity under a higher temperature environment (i.e., 60℃) over a shorter duration are comparatively smaller in magnitude when compared to the drying shrinkage under a lower temperature environment (i.e., 38℃) over a longer duration.

- The rate of mass loss from concrete is significantly higher compared to that of dry shrinkage. Consequently, even a minimal quantity of dry shrinkage leads to a considerable reduction in the mass of the concrete. Moreover, as concrete maturity increases, the extent of drying shrinkage and mass loss becomes increasingly clear. Significantly, the drying shrinkage behaviour slightly affects the development of the dynamic elastic modulus of concrete because this property is mainly restrained by aggregate components. Also, an inverse relationship is observed between relative humidity and porosity, whereby higher relative humidity is correlated with a decrease in both porosity and drying shrinkage.
- At the aspect of microstructure assessment, DRI numbers become greater when the concrete is exposed to conditions with low relative humidity. Meanwhile, when the concrete specimens with the same concrete maturity obtained the closed magnitude of drying shrinkage, their DRI number can be determined in a certain range. Significantly, when the level of concrete maturity is low, the primary factor responsible for causing damage to the concrete is the typical CCP that does not connect to the pores or ITZ. Nevertheless, the roles of pores and ITZ become of greater importance in the formation of CCPs at the high concrete maturity.
- The development of CCP induced by drying shrinkage does not only perform as the dispersion from the small part to the whole surface but also can be attained as high damage induced by the high concentration of CCP within one cell of the concrete polished surface. At low concrete maturity, drying shrinkage generates more CCPs in concrete at the identical magnitude of the length change of the expansion as decreasing relative humidity from the saturated condition. Meanwhile,

the similar magnitude of drying shrinkage causes a similar amount of CCPs. Significantly, the effect of drying shrinkage occurring at the low concrete maturity (i.e., 38°C) focused on the generation of more initial CCPs; also, the effect of drying shrinkage occurring at the high concrete maturity (i.e., 60°C) focuses on developing the existing CCPs.

Some recommendations are presented as follows:

- The reduction in mass seen in this study is influenced not only by the phenomenon of drying shrinkage but also by the degree of hydration. The hydration reaction process leads to a reduction in the volume of capillary pores, which are the main locations of drying shrinkage occurring in concrete. This reduction contributes to the development of concrete strength over time. In contrast, drying shrinkage continues to increase reducing the stiffness and strength of concrete over time. Hence, it is suggested to assess the degree of hydration in drying shrinkage concrete and understand the relationship between hydration and drying shrinkage influencing the mechanical properties of concrete.

- The thin and slender characteristics of CCPs generated by drying shrinkage make them difficult to observe under a magnification of 16x. The identification of separated or connected CCPs within the ITZ can provide challenges. Thus, the recommendations are made to the DRI procedure. 1) Checking the CCP while using a high magnification level of 20x, considering the different types of CCP and solving if CCP surrounds or hides in the ITZ and pores, 2) confirming the condition of the CCP by reverting to a magnification level of 16x, as the concept of DRI based on crack observations at this specific magnification.

- To ensure the precision of the DRI number, it is necessary to measure a specimen multiple time, commonly at least twice. Consequently, the specimens are frequently moved to the ambient environment from their respective exposure conditions for DRI. Nevertheless, the rate of development of CCPs caused by drying shrinkage is observed to be quicker than the theoretical amount of CCP due to variations in temperature and relative humidity within the laboratory. Consequently, it is recommended that, upon completion of the drying shrinkage measurement, the specimen should return to its exposure conditions instead of being sealed and stored in the laboratory.